

MULTIMODAL TUMOR IMAGING BY IRON OXIDES AND
QUANTUM DOTS FORMULATED IN POLY (LACTIC ACID)-D-
ALPHA-TOCOPHERYL POLYETHYLENE GLYCOL 1000
SUCCINATE NANOPARTICLES

TAN YANG FEI

NATIONAL UNIVERSITY OF SINGAPORE
2010

MULTIMODAL TUMOR IMAGING BY IRON OXIDES AND
QUANTUM DOTS FORMULATED IN POLY (LACTIC ACID)-D-
ALPHA-TOCOPHERYL POLYETHYLENE GLYCOL 1000
SUCCINATE NANOPARTICLES

TAN YANG FEI
(B.Eng. (Hons.), NUS)

A THESIS SUBMITTED
FOR THE DEGREE OF MASTER OF ENGINEERING
DEPARTMENT OF CHEMICAL AND BIOMOLECULAR ENGINEERING
NATIONAL UNIVERSITY OF SINGAPORE
2010

ACKNOWLEDGEMENTS

First of all, I would like to express my deep appreciation and gratitude towards the following people who have helped me to complete the thesis.

A big thank you to my research project supervisor, Professor Feng Si-Shen, for offering me an opportunity to be part of his Chemotherapeutic Engineering research group. I want to thank him for his invaluable support, both physically and morally, and all the guidance throughout the course of study.

All the professional officers and lab technologists, Mr. Chia Phai Ann, Dr. Yuan Ze Liang, Mr. Boey Kok Hong, Ms. Lee Chai Keng, Ms. Chew Su Mei, Ms. Samantha Fam, Ms. Alyssa Tay, Ms. Dinah Tan, Ms. Li Xiang, Mdm. Priya, Mdm. Li Fengmei, and many other staff from Laboratory Animal Centre (LAC) who have unconditionally helped in various kinds of administrative works as well as experiments and have willingly shared their knowledge and expertise to further enhance my learning process.

My dear colleagues, Mr. Prashant, Dr. Sneha Kulkarni, Mr. Liu Yutao, Mr. Phyo Wai Min, Ms. Chaw Su Yin, Mr. Mi Yu, Ms. Zhao Jing and all the final year students for all their kind assistances and supports they provided especially Ms. Wang Sui.

PUBLICATION

A journal with the same title as this thesis was published based on this work in Elsevier under Biomaterials. I am the first author of the published journal. Below is the relevant article information:

Multimodal tumor imaging by iron oxides and quantum dots formulated in poly(lactic acid)-D-alpha-tocopheryl polyethylene glycol 1000 succinate nanoparticles.

Biomaterials. 32;2011:2969-2978

Authors : Yang Fei Tan, Prashant Chandrasekharan, Dipak Maity, Cai Xian Yong, Kai-Hsiang Chuang, Ying Zhao, Shu Wang, Jun Ding and Si-Shen Feng

Received : 10 Dec 2010

Accepted : 31 Dec 2010

Available online : 22 Jan 2011

TABLE OF CONTENTS

ACKNOWLEDGEMENTS	i
PUBLICATION	ii
TABLE OF CONTENTS	iii
SUMMARY	v
LIST OF TABLES	x
LIST OF FIGURES	xi
LIST OF ABBREVIATIONS	xv
CHAPTER 1: INTRODUCTION	1
1.1 Background	1
1.2 Objectives and Scope	3
CHAPTER 2: LITERATURE REVIEW	4
2.1 Cancer Facts	4
2.2 Causes of Cancer	5
2.3 Molecular Imaging	7
2.4 How Molecular Imaging Works.....	8
2.5 Molecular Imagers in Radiotherapy (RT)	9
2.6 Current Imaging Techniques	10
2.7 Magnetic Resonance Imaging (MRI).....	11
2.8 MRI Contrast Agents	16
2.9 Superparamagnetic Iron Oxide (IO).....	17
2.10 Fluorescence Imaging	18
2.11 Fluorescence Imaging Principle	19
2.12 Quantum Dots (QDs)	21
2.13 Optical Properties of Quantum Dots (QDs)	21
2.14 Applications of Quantum Dots (QDs).....	22
2.15 Limitations of Quantum Dots (QDs).....	24
2.16 Challenges of QDs and IO application in Imaging	25
2.16.1 Insufficient Probes at Imaging Site	25
2.16.2 Cytotoxicity	30
2.17 Nanotechnology in Molecular Imaging.....	33
2.18 Multi-modality	34
CHAPTER 3: MATERIALS & METHODS	41
3.1 Materials.....	41
3.2 Synthesis Methods.....	42
3.2.1 Flocculation of QDs	42
3.2.2 Formulation of QDs and IOs-loaded NPs	42
3.3 Characterization of QDs and IOs-loaded NPs:	43
3.3.1 Particle Size and Size Distribution	43
3.3.2 Surface Charge	43
3.3.3 TEM Analysis.....	43
3.3.4 QDs and IOs Encapsulation Efficiency	43
3.3.5 XPS.....	44
3.4 Cell Line Experiment	45
3.4.1 Cell Cultures	45

3.4.2	In vitro cellular uptake of NPs.....	45
3.4.3	In vitro Cytotoxicity	46
3.5	Animal Study.....	47
3.5.1	Tumor imaging (MRI).....	47
3.5.2	Tumor Imaging (Fluorescent Imaging)	48
3.5.3	Biodistribution.....	49
CHAPTER 4: RESULTS & DISCUSSIONS		50
4.1	Characterization of QDs and IOs-loaded nanoparticles.....	50
4.1.1	Size and Size Distribution	50
4.1.2	Surface Charge	50
4.1.3	TEM Analysis.....	51
4.1.4	QDs and IO Encapsulation Efficiency	52
4.1.5	XPS.....	52
4.2	Cell Line Experiment	58
4.2.1	In vitro cellular uptake of NPs.....	58
4.2.2	In vitro Cytotoxicity	62
4.3	Animal Study.....	64
CHAPTER 5: OUTLOOK		72
CHAPTER 6: CONCLUSION		74
CHAPTER 7: REFERENCES.....		80
CHAPTER 8: APPENDIX.....		86

SUMMARY

Cancer has become the top killer of Man in recent decades. Thus, effective cancer detection is crucial as cancer can be easily tackled at its early stages. Molecular imaging enables the detection of a disease in its earliest stage. Three medical imaging techniques often used in the current clinical practice are the X-ray computed tomography (CT), positron emission tomography (PET) and magnetic resonance imagery (MRI). CT and PET scans involve radiation exposures. Hence, the non-invasive MRI is preferred.

To provide a better contrast in MRI, contrast agents are introduced. Superparamagnetic iron oxide (IO) is widely used as a contrast agent for MRI. It exhibits excellent magnetic properties and acceptable biocompatibility. IO can vastly enhance imaging due to its exceptional penetration depth. Furthermore, it has zero retained magnetism after the removal of magnetic field. Another probe used for amplification strategy is quantum dots (QDs) as luminescence probes in fluorescence imaging. Advantages of fluorescence imaging includes high sensitive detection, multicolor detection, probe stability, low hazard and low cost. Contrast agents such as organic fluorescent dyes and Quantum Dots (QDs) are often used to promote fluorescence imaging. Quantum dots (QDs) are composed of atoms from groups II-VI or III-V of the periodic table. Their advantages include *in vivo* longevity and tunable emission from visible to infrared wavelength by changing the size and composition of QDs. QDs also have broad excitation spectra with high absorption coefficients, high quantum yield of fluorescence, strong brightness, high resistance to photobleaching and good sensitivity.

Although necessary, amplification strategies are not enough to produce high quality images. Sufficient concentrations of probes must be gathered at the intended imaging

area for an adequate period *in vivo*. Nevertheless, the agent dose is limited by the side effects of the agent and the rapid removal of probes from the blood system due to the body's mononuclear phagocyte system (MPS) interactions after opsonization. A method to cloak nanoparticles from MPS recognition is the surface modification of the probes to prevent opsonin proteins in the blood from being attached to the particles surfaces. Generally, hydrophilic particles opsonize slower than hydrophobic particles and neutrally charged particles opsonize slower than charged particles. Till date, the most effective and most commonly used polymers as shielding groups are the PEG-containing copolymers. One important example of such a copolymer is poly (lactic acid)-D-alpha-tocopheryl polyethylene glycol 1000 succinate (PLA-TPGS) that is gaining popularity in the research scene today.

Certain probes may have very good affinity with certain targets of imaging interest however they may pose to be toxic to the body. To use such probes, encapsulation via PEGylation may be needed to reduce cytotoxicity. Another method to decrease cytotoxicity is by targeted delivery. Targeting is divided into passive and active targeting. In passive targeting, nanoparticles accumulate at the tumor through the enhanced permeability and retention (EPR) effect. The vascular structures of tumors are defective and lack effective lymphatic drainage system, causing particles to accumulate in them. Passive targeting is the prime objective for our probe system to achieve.

Molecular imaging requires high affinity probes with reasonable pharmacodynamics. Such probes are usually nanoparticles. Synthesizing imaging probes into nanoparticles not only aids in escaping MPS detection but also increases cellular uptake. Thus, the formulation of imaging probes such as IOs and QDs in

nanoparticles of biodegradable polymers may provide an ideal solution to reduce toxicity as well as enhance cellular uptake, hence improving imaging effects.

IO and QD probes are effective probes for amplification in molecular imaging. However, individual imaging probes have their advantages and disadvantages. For instance, IO probes provide high spatial resolution and unlimited depth penetration but their sensitivity in imaging fails in comparison to optical fluorescence imaging probes such as QDs. QDs, in turn; have excellent imaging effects and long half-life, but their ability for tissue penetration is limited due to the refraction and adsorption of light in the living organism. Therefore, it is very important to find an imaging method that can fulfill the requirements in medical applications as much as possible, and this can be achieved by applying multi-modal imaging.

Multi-modal imaging means applying two or more imaging modalities concurrently. Multimodal imaging can be developed to make use of the advantages and overcome the limitations, which can be realized by co-encapsulation of QDs and IOs in ligand-conjugated nanoparticles of biodegradable polymers. To achieve a thorough analysis of one multi-modal imaging system, *in vivo*, *ex vivo* and *in vitro* analyses should be done and cross-referenced. Most studies in the research field are related to either *ex vivo* or *in vitro* analysis, lacking in *in vivo* analysis. In addition, some imaging modalities such as CT imaging have significant side effects on human health. Both fluorescence imaging and MRI will not cause radiation injury. On top of that, QDs and IO as contrast agents have been widely studied in biomedical applications. Therefore, encapsulating both QDs and IO in PLA-TPGS copolymers, as multi-modal imaging probes should provide high quality images. This probe should have high sensitivity and depth penetration.

This thesis illustrates a multimodal imaging system developed by co-encapsulating superparamagnetic iron oxides (IOs) and quantum dots (QDs) in the nanoparticles (NPs) of poly (lactic acid) - d- α -tocopheryl polyethylene glycol 1000 succinate (PLA-TPGS) for use in both magnetic resonance imaging (MRI) and fluorescence imaging. This multimodal imaging system not only combines the advantages of both MRI and fluorescence imaging, but also overcomes their disadvantages. This imaging system also promotes sustained and controlled imaging with passive targeting effects to the diseased cells. The QDs and IOs-loaded PLA-TPGS NPs were prepared by a modified nanoprecipitation method, which were then characterized for their size and size distribution, zeta-potential and the imaging agent encapsulation efficiency. The transmission electron microscopy (TEM) images showed direct evidence for the well-dispersed distribution of the QDs and IOs within the PLA-TPGS NPs. The cellular uptake and the cytotoxicity of the PLA-TPGS NPs formulation of QDs and IOs were investigated *in vitro* with MCF-7 breast cancer cells, which were conducted in close comparison with the free QDs and IOs at the same agent dose. To investigate the biodistribution of the QDs and IOs-loaded PLA-TPGS NPs among the various organs, animal studies were conducted where mice cultivated with MCF-7 breast cancer tumors were injected with the developed NPs. The results showed greatly enhanced tumor imaging due to the passively targeting effects of the NPs to the tumor. Images of tumors were acquired *in vivo* by a 7T MRI scanner. Further *ex vivo* images of the tumors were obtained via confocal laser scanning microscopy. Such a multimodal imaging system shows great advantages of both contrast agents making the resultant probe highly sensitive with good depth penetration. A subject administered with the developed NPs can undergo both MRI and fluorescence imaging. Any imagery feature detected in one imaging picture which may suggest any disease or tumor

growth, can be further compared and confirmed with the imaging picture taken by the other imaging technique.

LIST OF TABLES

Table	Description	Page no.
4.1	Characteristics of the QDs and IOs-loaded PLA-TPGS nanoparticles including particle size and polydispersity (PDI), zeta potential (ZP) and encapsulation efficiency percentage (EE%).	51

LIST OF FIGURES

Figure	Description	Page no.
2.1	Cancer formation through mutations.	5
2.2	Causes of cancer.	7
2.3	CT imager.	10
2.4	PET imager.	11
2.5	MRI.	12
2.6	Zeeman effect.	13
2.7	(A): A collection of H nuclei in the absence of an externally applied magnetic field. (B): An external magnetic field B_0 is applied which causes the nuclei to align themselves in one of two orientations with respect to B_0 (denoted parallel and anti-parallel).	14
2.8	At Larmor frequency, the net magnetization flips 90° and the spins are whipped to precess in phase.	15
2.9	Axial T1 weighted (A) and T2 weighted (B) images of the brain magnetic resonance imaging (MRI) demonstrating a lacunar infarction (arrow).	17
2.10	IVIS Fluorescence imager.	19
2.11	Jablonski diagram illustrating the processes involved in creating an excited electronic singlet state by optical absorption and subsequent emission of fluorescence. ①:Excitation; ②:Vibrational relaxation; ③:Emission.	20
2.12	Excited quantum dots arranged according to size.	22
2.13	QDs applications.	23
2.14	CdSe QDs release of toxic Cd^{2+} ions by photolysis under UV illumination.	24
2.15	Opsonization and Phagocytosis of a bacteria.	26
2.16	<i>In vitro</i> MRI of commercial IO (Resovist) and IO-loaded PLGA-mPEG nanoparticles suspended in water (TE=7ms).	29
2.17	Passive and active tumor targeting.	32

2.18	Schematic illustration of the multi-functional HSA-IONPs. The pyrolysis-derived IONPs were incubated with dopamine, after which the particles became moderately hydrophilic and could be doped into HSA matrices in a way similar to drug loading.	35
2.19	Synthesis of hybrid silica nanoparticles.	37
2.20	Schematic illustration of MFR-AS1411 synthesis. MF particles had carboxyl group and Fmoc-protected amine moiety, which was coupled with amine terminated AS1411 aptamer using EDC (MF-AS1411). After reaction of MFAS1411 with p-SCN-bn-NOTA, particles were reacted with ⁶⁷ Ga-citrate to form MFR-AS1411.	38
4.1	TEM Images of A: the IOs-loaded PLA-TPGS NPs, B: the QDs-loaded PLA-TPGS NPs and C: the QDs and IOs-loaded PLA-TPGS NPs (scale bar = 200 nm).	51
4.2	Particle XPS result for Cd showing no peaks (absence of Cd).	53
4.3	Grinded particle XPS for Cd showing 2 peaks (presence of Cd).	54
4.4	Particle XPS result for Se showing no peaks (absence of Se).	54
4.5	Grinded particle XPS for Se showing 1 peak (presence of Se).	55
4.6	Particle XPS result for Zn showing no peaks (absence of Zn).	55
4.7	Grinded particle XPS for Zn showing 2 peaks (presence of Zn).	56
4.8	Particle XPS result for Fe showing no peaks (absence of Fe).	57
4.9	Grinded particle XPS for Fe showing 2 peaks (presence of Fe).	57
4.10	CLSM images of MCF-7 cells treated with the QDs and IOs-loaded PLA-TPGS NPs <i>in vitro</i> (scale bar = 10 μm). A: Bright field image of cells. B: Blue coded DAPI stained nuclei. C: Red coded QD from NPs in cytoplasm. D: Complete overlapped image.	59
4.11	Cellular uptake efficiency of the MCF-7 cancer cells after 1, 2 and 4 h treatment with 100 μL of the QDs and IO-loaded PLA-TPGS NPs of concentrations containing 1 μg/mL Cd, 0.5 μg/mL Cd and 0.25 μg/mL Cd respectively dispersed in medium.	61

4.12	<i>In vitro</i> viability of MCF-7 cells after 24 and 48 hour treatment with the free IO, the free QDs (containing 1.42 µg/mL Cd), the free IO (containing 5.73 µg/mL Fe), and the QDs and IOs-loaded PLA-TPGS NPs (containing 1.42 µg/mL Cd and 5.73 µg/mL Fe) respectively dispersed in the medium.	63
4.13	Axial MRI image sections of the MCF-7 grafted tumor bearing mice. Images A and B show the part of the tumor (shown by the arrow) before and after 6 hours of administration of the QDs and IOs-loaded PLA-TPGS NPs into the mice. Images C and D show the kidney (K) and liver (L) part of the mice before and 6 hours after the administration of the PLA-TPGS NPs formulation of QDS and IOs (dosage: 1.5 mg of Cd/kg of body weight or equivalent of 6.0 mg of Fe/kg body weight). The decrease in intensity in the regions of the tumor and liver can be noticed in comparison with the color scale shown aside.	64
4.14	Fluorescent Images of the various organs. Upper row: control. Lower row: Organs of the mouse treated with the QDs and IOs-loaded PLA-TPGS NPs (dosage: 1.5 mg of Cd/kg of body weight or equivalent of 6.0 mg of Fe/kg body weight).	66
4.15	Fluorescence intensity increase percentage for the various organs of the mice treated with the QDs and IOs-loaded PLA-TPGS NPs (dosage: 1.5 mg of Cd/kg of body weight or equivalent of 6.0 mg of Fe/kg body weight).	67
4.16	Confocal laser scanning microscopy sections of the mouse liver (scale bar = 60 µm). Images A, B and C show the liver sections of the control with no treatment. A: Blue coded DAPI stained nuclei. B: Red channel detection showing no signal due to absence of QDs. C: Complete overlapped image of A and B. Images D, E and F show the liver sections of the mouse treated with the QDs and IOs loaded PLA-TPGS NPs. D: Blue coded DAPI stained nuclei. E: Red coded QD from NPs in cytoplasm. F: Complete overlapped image.	68
4.17	Confocal laser scanning microscopy sections of the mouse kidney sections (scale bar = 60 µm). Images A, B and C show the kidney sections of the control with no treatment. A: Blue coded DAPI stained nuclei. B: Red channel detection showing no signal due to absence of QDs. C: Complete overlapped image of A and B. Images D, E and F show the kidney sections of the mouse treated with the QDs and IOs loaded PLA-TPGS NPs. D: Blue coded DAPI stained nuclei. E: Red coded QD from NPs in cytoplasm. F: Complete overlapped image.	69

4.18	<p>Confocal laser scanning microscopy sections of the mouse tumor sections. Images A, B and C (scale bar = 30 μm) show the tumor sections of the control with no treatment. A: Blue coded DAPI stained nuclei. B: Red channel detection showing no signal due to absence of QDs. C: Complete overlapped image of A and B. Images D, E and F (scale bar = 20 μm) show the tumor sections of the mouse treated with the QDs and IOs loaded PLA-TPGS NPs. D: Blue coded DAPI stained nuclei. E: Red coded QD from NPs in cytoplasm. F: Complete overlapped image.</p>	70
------	--	----

LIST OF ABBREVIATIONS

Abbreviation	Description
ADME	Absorption, distribution, metabolism and excretion
As	Arsenic
Cd	Cadmium
CLSM	Confocal laser-scanning microscope
cps	Counts per second
CT	X-ray computed tomography
Cu	Copper
DAPI	4,6-Diamidino-2-phenylindole dihydrochloride
DI	Deionized
DMSO	Dimethyl sulfoxide
DNA	Deoxyribonucleic acid
EDTA	Ethylenediaminetetraacetic acid
EE	Encapsulation efficiency
Er	Erbium
EPR	Enhanced permeability and retention
F	Fluorine
FBS	Fetal bovine serum
FDA	Food and drug administration
Fe	Iron
Ga	Gallium
Gd	Gadolinium
HA	Hydroxyapatite
HLB	Hydrophile lipophile balance
ICP-MS	Inductively coupled plasma mass spectrophotometer
In	Indium
InC	Fluorescence intensity of cells in control wells
InS	Fluorescence intensity of cells in sample wells
IO	Iron oxide
LLS	Laser light scattering
MDR	Multiple Drug Resistance
Mn	Number averaged molecular weight
mPEG	Methyl polyethylene glycol
MPS	Mononuclear phagocyte system
MRI	Magnetic resonance imagery
ms	Milli second
MTT	Methylthiazolyldiphenyl-tetrazolium bromide

Mz	Net magnetization
N	Nitrogen
Na	Sodium
NIRF	Near-infrared imaging
NMR	Nuclear magnetic resonance spectroscopy
NP	Nanoparticle
O	Oxygen
PBS	Phosphate buffered saline
PDI	Poly Dispersity Index
PEG	Polyethylene glycol
PET	Positron emission tomography
PLA	Poly (lactic acid)
PLA-TPGS	Poly (lactic acid)-D-alpha-tocopheryl polyethylene glycol 1000 succinate
PLEA	Poly (lactic acid)-poly (ethylene glycol)
PLGA	Poly (lactic-co-glycolic acid)
QD	Quantum dot
RES	Reticuloendothelial system
RF	Radio frequency
ROI	Region of interest
RT	Radiotherapy
Ru	Ruthenium
S	Sulphur
SCID	Severe combined immunodeficiency
Se	Selenium
Si	Silica
SWNT	Single walled carbon nano tube
T1	Longitudinal relaxation time
T2	Transverse relaxation time
Te	Tellurium
TE	Echo delay time
TEM	Transmission electron microscope
THF	Tetrahydrofuran
Tm	Thulium
TR	Repetition time
UV	Ultra violet
XPS	X-ray photoelectron spectroscopy
Yb	Ytterbium
ZP	Zeta potential
Zn	Zinc

CHAPTER 1: INTRODUCTION

1.1 Background

Cancer is the result of the uncontrolled growth and spreading of abnormal cells (Feng SS and Chien S, 2003). Cancer cells can spread in the body through the blood and lymph systems (<http://www.cancer.gov/cancertopics/what-is-cancer>). Cancer is the leading cause of death in various developed countries. In the United States, there were about 1,529,560 new cases of cancers reported in 2010. On top of that, cancer associated death cases amounted to an alarming 569,490 in the very year (<http://www.cancer.gov/cancertopics/what-is-cancer>). Therefore, it is evidently important to find efficient ways to combat cancer.

Massive advancements have actually been made in cancer treatments as compared to the last decade. However, developments in molecular imaging systems to detect cancer witnessed rather sluggish progress. Molecular imaging is an *in vivo* characterization and measurement of the disease process at the cellular and molecular level, which aims at investigating cellular functions without disturbance. In actual fact, in order to effectively overcome cancer, it is of paramount importance to first efficiently detect them. This is because, just like any other diseases, cancers can be easily and effectively treated in their early stages especially before tumors metastasize. Developing an advanced imaging system to detect cancer can realize this. In recent years, researchers have finally realized the importance of advancing imaging techniques resulting in great interests in advanced cancer imaging systems. Scientists expected that by using efficient cancer imaging techniques, the stage and precise locations of cancer could be determined efficiently. Apart from that, cancer imaging can also aid cancer treatment especially during operations and help monitor the

treatment effects (<http://imaging.cancer.gov/imaginginformation/cancerimaging>).

Thus, an effective cancer imaging system is highly in demand.

In order to enhance molecular imaging, contrast agents are utilized as imaging probes. Contrast agents make molecular imaging possible and effective by enhancing the image contrast between healthy and abnormal tissues. Thus, they are needed for many imaging techniques. However, most contrast agents have some toxicity issues and are thus not biocompatible. Besides causing some side effects in the human body due to the toxicity, some contrast agents may have cell uptake limitation and could not be efficiently delivered into cells. On top of that, human immune system detection of these foreign contrast agents may also cause circulation limitations. Therefore, it is crucial to find a better way to control deliver the contrast agents into human cells while decreasing their cytotoxicity. Researchers found that by modifying contrast agents into nanoparticles, advantages such as the desired control delivery system, long vascular half-life and fewer side effects on human body can be achieved. In doing so, the imaging quality can be increased and it will be easier for doctors to find the accurate position of cancer in the body, locate the extent of cancer spreading, identify specified cancer treatment and monitor the effect of the treatment.

Although contrast agents could enhance molecular imaging, every individual contrast agents have its advantages and limitations. Therefore, by only using one contrast agent and utilizing one mode of imaging may result in certain features within organs suggesting the onset of a particular disease to be overlooked. Therefore, the idea of dual modality was born which involves combining two contrast agents into a single probe. One dosage of this probe enables the patient to undergo two modes of imaging techniques. The results of the imaging can then be analyzed concurrently. This acts as

a more effective imaging practice to ensure no diseases get overlooked and left to develop into tricky late stages where treatment may be complicated.

1.2 Objectives and Scope

The main objective of this project is to encapsulate both quantum dots (QDs) and superparamagnetic iron oxide (IO) in biodegradable copolymer PLA-TPGS. Basic characterization studies will be conducted on the nanoparticles to investigate the particle size, polydispersity, surface charge and encapsulation efficiency. Cell line work will be conducted using the nanoparticles. Cell studies include cell uptake and cell toxicity experiments. On top of that, bio distribution experiments will be conducted on treated cancer induced animals. Finally, molecular imaging will also be used on animals treated with the particles.

CHAPTER 2: LITERATURE REVIEW

2.1 Cancer Facts

Cancer is currently the leading cause of death globally. According to the US National Cancer Institute, cancer is defined as a category of affiliated diseases whereby abnormal cells go through uncontrolled transformation (or mitosis) and have the ability to spread to other parts of the body via the blood circulation and lymphatic systems (metastasis).

In the normal state, cells grow and replicate to form new cells according to the needs of the body. Whenever cells grow old and die, new cells replace them. However at times, this ideal orderly process goes wrong in which new cells form when the body does not need them, and old cells do not die when they should. The resultant extra cells gather to form a mass of tissue. This mass is known as a tumor. Tumors can be either benign (non cancerous) or malignant (cancerous). Benign tumors are localized and do not spread to other parts of the body. They are rarely life threatening. Malignant tumors, on the other hand, can spread (metastasize) and may be life threatening (<http://www.cancer.gov/cancertopics/what-is-cancer>).

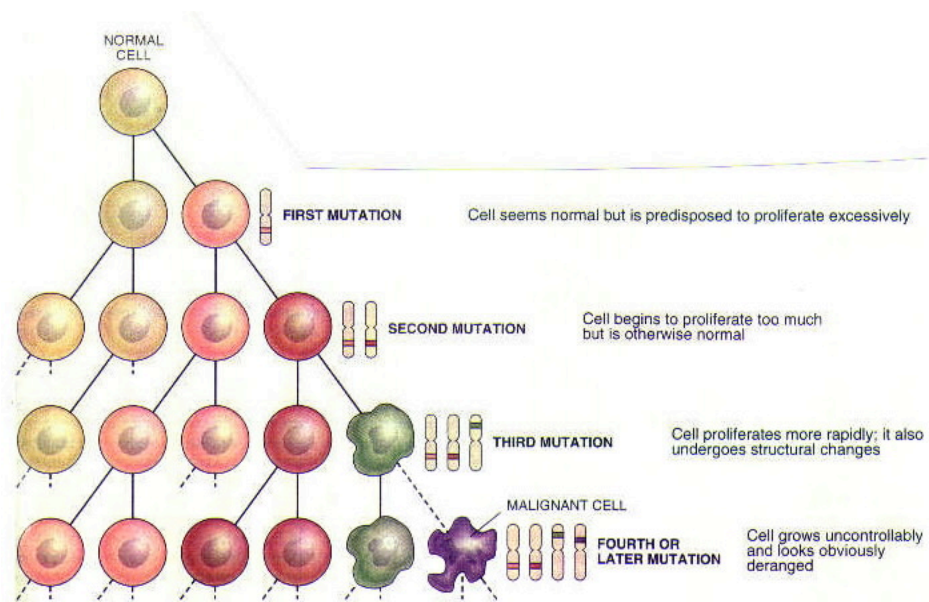


Figure 2.1: Cancer formation through mutations.

(Adapted from <http://www.chemcases.com/cisplat/cisplat19.htm>)

A projection from statistics revealed that for every three people, one would be diagnosed with cancer in his lifetime. On top of that, occurrences rate of cancer are increasing at a rate of 1% per year (<http://news.bbc.co.uk/2/hi/health/3444635.stm>). Till today, more than 200 different types of cancer have been discovered. The probability of getting cancer is distinct in different types of tissues or organs, even within the same individual.

2.2 Causes of Cancer

There are various causes for cancer. These causes can basically be subdivided into two categories, namely the intrinsic and extrinsic factors. Intrinsic factors mainly include the genetic make up of the body and the individuals cannot control this. It implies that once a person is born, the genetic make up has already been coded to determine the number of genetic mutations he or she will experience in the lifetime.

Some of these mutations may ultimately lead to cancer. The causes of such mutations include inheritance from previous generations, abnormal fertilization or improper fetal developments during pregnancy. Mutations may not always result in cancer. However, inheritance of certain harmful gene mutations may increase the risk of cancer development. For instance, research has shown that women who inherited harmful BRCA1 and BRCA2 gene mutations can have a very higher risk of developing breast cancer in their lifetime as compared to those who did not inherit such gene mutations (<http://www.cancer.gov/cancertopics/factsheet/Risk/BRCA>).

In general, extrinsic factors play a bigger role in determining the development of cancer. Extrinsic factors encompass a wide variety of causes, ranging from environmental factors to the individual's personal daily lifestyle. Daily lifestyle practices such as diet directly influences the risk of getting cancer. Preservatives such as nitrosamine, nitrosamide, sulphites as well as colorings, which are usually added during food processing, can potentially accumulate in the body over an extended period of time and cause cancer (<http://www.cfsan.fda.gov/~dms/fdpreser.html>; <http://www.nswcc.org.au/editorial.asp?pageid=2345>). Genetically-modified food (staples such as rice and potatoes included) as well as food rich in methyl donors has been reported to be able to potentially trigger genetic mutations, stimulating tumor growth (Watters, 2006; <http://www.independent.co.uk/life-style/health-and-wellbeing/health-news/suppressed-report-shows-cancer-link-to-gm-potatoes-436673.html>). Besides dietary habits, harmful habits such as smoking and drinking are also major factors causing cancers. For instance, more than 38,000 people are diagnosed with lung cancer every year. Of these deaths, almost 90% is tobacco related (<http://info.cancerresearchuk.org/cancerstats/types/lung/?a=5441>).

As the average human life span increases with groundbreaking discoveries in the

medical arena, mutations in cells and tissues are given enough time to develop into cancer. On top of that, industrializations globally, increased radiation due to ozone damage, extensive production of processed food and various failing personal lifestyle has raised the risk of various cancers in the present human population. Therefore, it is important to guard against cancer and the first step in doing so would be to do molecular imaging periodically to detect any preliminary onset symptoms of cancer.

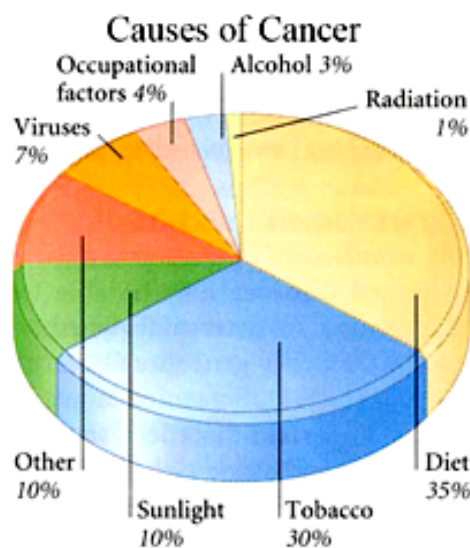


Figure 2.2: Causes of cancer.

(Adapted from <http://www.dmacdigest.com/cancer.html>)

2.3 Molecular Imaging

Early stage diagnosis plays a key role in determining the prognosis for diseases, especially for fatal ailments such as cancer and cardiovascular diseases. Molecular imaging provides critical information necessary to diagnose a disease in its earliest stage, which is an *in vivo* characterization and measurement of the disease process at the cellular and molecular level. Its objective is to investigate molecular basis and diagnose abnormalities of cellular functions as well as follow up molecular processes

in living organisms in a non-invasive way. Development of novel agents, signal amplification strategies, and imaging technologies have been extensively made with prior research efforts to improve molecular imaging.

Currently, the assessment of disease is based on anatomic or physiologic changes that are a late manifestation of the molecular changes that truly underlie disease. Direct imaging of these molecular changes will improve patient care by allowing earlier detection of diseases such as cancer, neurological and cardiovascular diseases. It may be possible to image molecular changes, allowing intervention at a time when the outcome is most likely to be affected. In addition, by directly imaging the underlying alterations of disease, it will be possible to directly image the effects of therapy. Therefore, it will be possible to play a direct role in determining the effectiveness of treatment shortly after therapy has been initiated, in contradistinction to the many months often required today to determine whether intervention has been beneficial. Molecular imaging also contributes to improving the treatment of disorders by optimizing the pre-clinical and clinical tests of new medication.

To image specific molecules *in vivo*, various criteria must be met. These criteria are, availability of high affinity probes also known as biomarkers, the ability of these probes to overcome delivery barriers (vascular, interstitial, cell membrane), use of amplification strategies (chemical or biologic) and availability of sensitive, fast, high resolution imaging techniques (Weissleder R et al., 2001). All four factors must be met for successful *in vivo* imaging at the molecular level.

2.4 How Molecular Imaging Works

Basically, the probes interact chemically with their surroundings and in turn alter the image according to molecular changes occurring within the area of interest

(Weissleder R et al., 2001). This process is distinctly different from previous methods of imaging which primarily imaged differences in qualities such as density or water content. Some concerns for the design of the probes are their targeting ability to areas where imaging are needed and also their ability to cloak from the body's immune system before they reach the targeted site.

There are various modalities of molecular imaging available currently. Different imagers can be utilized for different stages of radiotherapy.

2.5 Molecular Imagers in Radiotherapy (RT)

A typical process of high-precision RT techniques consists of five major phases. They are simulation, treatment planning, set-up verification, beam delivery and response assessment. For simulation phase, the patient is immobilized according to treatment delivery. The patient's structural information is obtained. This information is then transferred to an RT planning system for the treatment-planning step in which tumor extension and organ at risks are identified with the target volume to be treated defined. Treatment parameters are determined according to the volumes defined on images and dose prescription. Once a plan that meets the criteria is calculated, the parameters of the plan are automatically transferred to the treatment machine. In the third phase, the patient is positioned on the treatment table for each treatment session in the same way as was done during the simulation. In the fourth phase, the beam delivery stage, the machine is operated according to the planned parameters. In selected cases, such as lung and liver lesions, this step can take advantage of real-time assessment of tumor position. Finally, the fifth phase regards the assessment of tumor response after RT, important in determining treatment success and in guiding future patient therapy (Michela L et al., 2008). Throughout the radiotherapy process, various

molecular imagers can be utilized. The focus of this paper will be the possible molecular imagers that can be utilized in the planning phase.

2.6 Current Imaging Techniques

Three medical imaging techniques, which are used most often in the current clinical practice, are the X-ray computed tomography (CT), positron emission tomography (PET) and magnetic resonance imagery (MRI). All these three imaging techniques involve using contrast agents.

In CT scans, radiocontrast agents are used. They are grouped into ionic and nonionic agents. As they are typically iodine compounds, adverse reactions are a concern. The risk for adverse reaction is 4% to 12% with ionic contrast materials and 1% to 3% with nonionic contrast materials (Cochran ST, 2005). Besides the potential risks from using the radiocontrast agents, CT scans also expose patients to harmful X-ray radiation.



Figure 2.3: CT imager.

(Adapted from <http://stardiagnosics.org/RADIOLOGY.HTML>)

On the same note, PET scans also involve the use of radioactive tracer isotopes to promote imaging. These radiotracers are extremely unstable and ionize, resulting in

radiation during imaging. In view of the radiation exposures of CT and PET scan, it is obvious that MRI is the preferred imagery technique, as it is non-invasive and will not cause radiation injury.



Figure 2.4: PET imager.

(Adapted from <http://www.fmh.org/body.cfm?id=155>)

2.7 Magnetic Resonance Imaging (MRI)

For the last three decades, magnetic resonance imaging (MRI) has been one of the more powerful imaging techniques for the examination of the human anatomy, physiology and pathophysiology largely due to the fact that it is non-invasive. Since its invention in 1973 by Paul Lauterbur, MRI has currently been widely used in

hospitals since its approval by the FDA for clinical use in 1985 (Yan GP et al., 2007). MRI images have excellent soft tissue specificity. It involves the use of a magnetic field, radio waves and a computer to produce detailed images of the body's interior, providing great soft tissue contrast that enables the differentiation between healthy and abnormal tissues (cancerous cells/tumors) (Jain TK et al., 2009).



Figure 2.5: MRI.

(Adapted from http://brainimaging.waisman.wisc.edu/facilities/ni_facilities.html)

The principle of MRI is based on the intrinsic properties of charge, spin and magnetism of the atomic nuclei (Jackson GD et al., 2005). The human body is largely composed of water molecules that contain two hydrogen nuclei or protons. When exposed to an external magnetic field, the energy of the nuclei will split into lower

(moment parallel with field) and higher (antiparallel) energy levels according to the Zeeman effect.

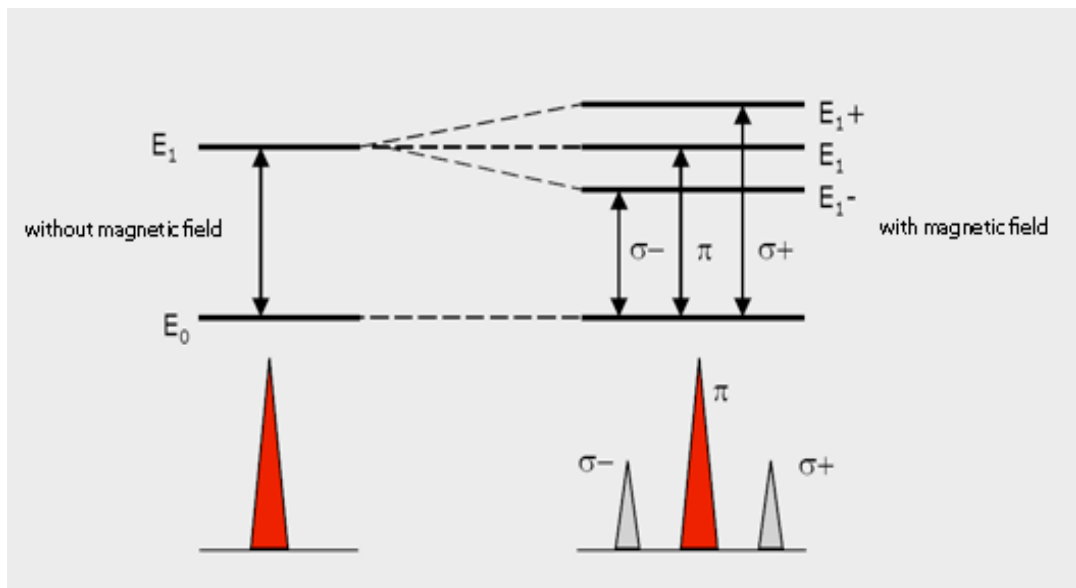


Figure 2.6: Zeeman effect.

(Adapted from http://www.msscien.com/aj/Fund_AAS/web/spectral-interferences-in-grap.161+m52087573ab0.0.html)

The parallel alignment is the preferred stable alignment. The energy difference between these two energy states corresponds to a very specific frequency necessary to excite a nucleus from the lower to the higher state. As a result of a larger number of nuclei in the parallel alignment, a net magnetization vector results.

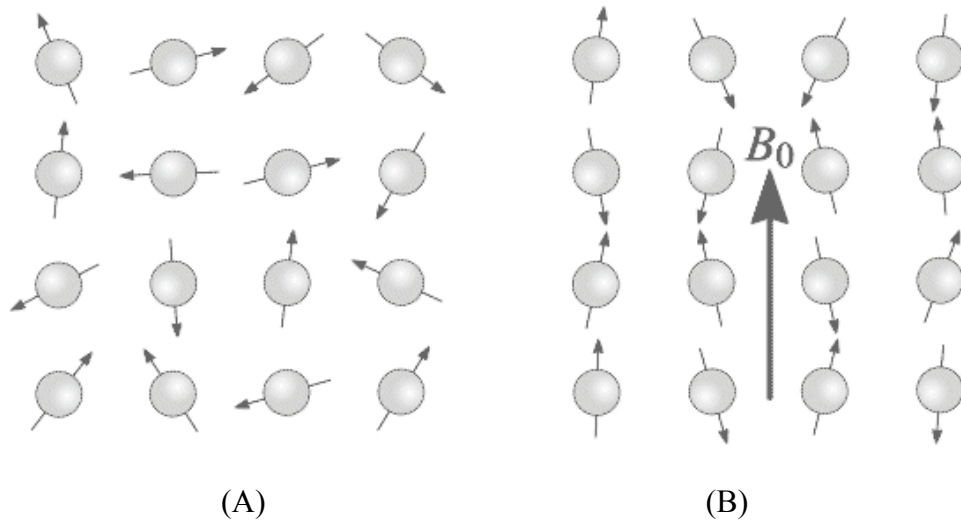


Figure 2.7: (A) A collection of H nuclei in the absence of an externally applied magnetic field. (B) An external magnetic field B_0 is applied which causes the nuclei to align themselves in one of two orientations with respect to B_0 (denoted parallel and anti-parallel).

(Adapted from <http://www.mikepuddephat.com/Page/1603/Principles-of-magnetic-resonance-imaging>)

When a radiofrequency (RF) pulse (equal to the Larmor frequency: the frequency of the precession of individual nuclei around the direction of the magnetic field) is applied, the protons would switch from the parallel state to the antiparallel state and the spins are forced to precess in phase. The net magnetization (M_z) flips 90° from the positive z-axis to the transverse plane.

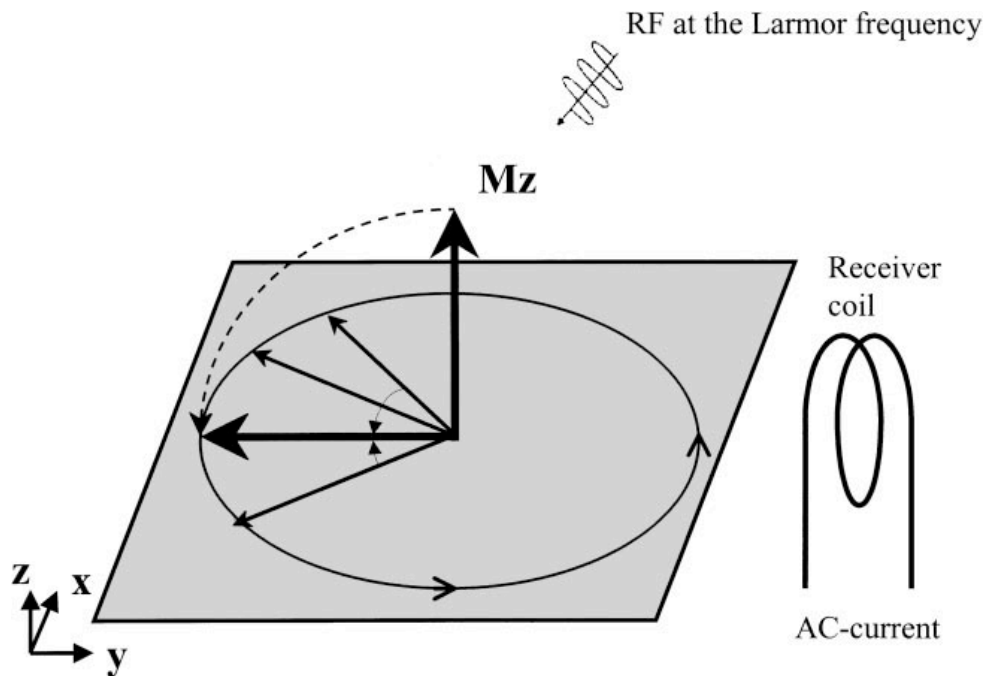


Figure 2.8: At Larmor frequency, the net magnetization flips 90° and the spins are forced to precess in phase.

After the radiofrequency pulse is lifted, the nuclei would go back to the initial equilibrium state and the time taken for this process is known as the relaxation time. There are two states of relaxation process: transverse and longitudinal. Longitudinal relaxation time (T_1) is the time required for the nuclei to realign to the external magnetic field and is defined as the time for the system to reach 63% of its equilibrium value after subjecting to a 90° RF pulse. On the other hand, transverse relaxation time (T_2) is the time required for 63% of the RF generated transverse magnetization to dissipate which occurs due to the dephasing of the spins. As a result of relaxation, the energy absorbed during the application of the RF pulse will be released in the form of a signal that can be detected by a receiver coil. Using a combination of RF pulses and magnetic field gradients, an MRI image can be obtained due to the variation in T_1 and T_2 values of different tissues that in turn give rise to the image contrast (Van Geuns RJM et al., 1999).

Although MRI is presently popular due to its noninvasive property, one drawback of MRI is its natural insensitivity of imaging for label detection. This can fortunately be overcome by using targeted MRI contrast agents coupled with biologic amplification strategies. One example is the cellular internalization of superparamagnetic probes such as monocrySTALLINE iron oxide nanoparticles (Moore A et al., 1998; Weissleder R et al., 2000).

2.8 MRI Contrast Agents

In order to provide a better contrast in MRI, contrast agents are introduced. MRI contrast agents are substances that enhance the image contrast between healthy and abnormal tissues. Most MRI contrast agents achieve that by altering the relaxation times of the water protons in places where the agents accumulate.

MRI contrast agents are split into two groups: T1-agents and T2-agents. T1-agents increase the longitudinal relaxation rates of protons more than the transverse relaxation rates. They reduce T1 relaxation time more than T2. Therefore, they tend to increase the signal intensity and make the MRI images appear brighter. Due to this effect, T1-agents are also known as positive contrast agents (Yan GP et al., 2007). Examples of T1-contrast agents are paramagnetic metals such as gadolinium, manganese and dysprosium. These free metals, in their ionic states, are not suitable contrast agents due to their toxicities and undesirable biodistribution. To utilize these agents, ligands must be treated with these metal ions to form chelates. In this way, kinetically stable complexes can be formed which can be excreted intact, decreasing their toxicity.

On the other hand, T2-agents increase the transverse relaxation rates more than the longitudinal relaxation rates. They reduce T2 relaxation time more than T1. The

signal intensity is reduced upon T2-agents applications and the MRI images appear darker. As a result, they are also known as negative contrast agents (Yan GP et al., 2007). Examples of T2-agents are superparamagnetic iron oxides.

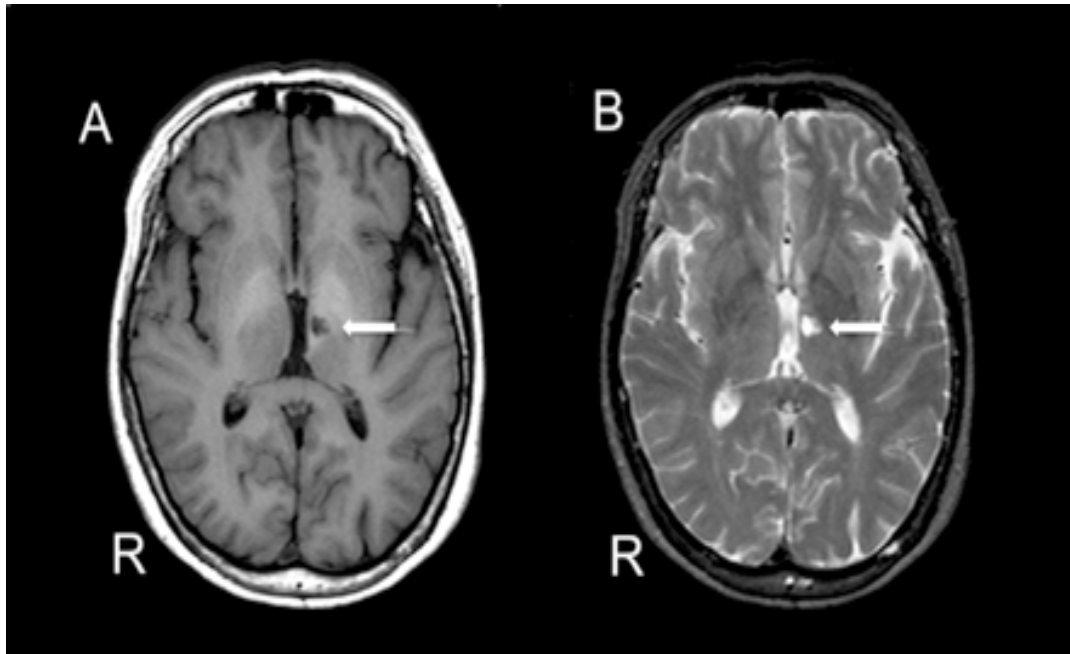


Figure 2.9: Axial T1 weighted (A) and T2 weighted (B) images of the brain magnetic resonance imaging (MRI) demonstrating a lacunar infarction (arrow).

(Adapted from <http://casereports.bmj.com/content/2009/bcr.04.2009.1754.full>)

2.9 Superparamagnetic Iron Oxide (IO)

Superparamagnetic iron oxide (IO) is widely used as a contrast agent for MRI. Most superparamagnetic iron oxides include cores consisting of iron oxides of 2-20 nm. They are usually made soluble and biologically stable via means of organic coatings. These organic coatings are commonly dextran or polyethylene glycol. As superparamagnetic IO is more effective in reducing T_2 relaxation time, the images obtained when using superparamagnetic IO particles as contrast agents will be darker at the parts where they accumulate (Sahana D et al., 2008).

When compared with other MRI contrast agents, superparamagnetic IO appears to be superior, exhibiting some favorable magnetic properties and acceptable biocompatibility. Firstly, it can vastly enhance imaging due to its exceptional penetration depth. Secondly, superparamagnetic IO has zero retained magnetism after the removal of magnetic field (Mu L et al., 2002). On top of that, its uptake by macrophages and migration to the lymph nodes also make them widely used for nodal staging (Molday RS et al., 1982). However, IO has some disadvantages, which limit their application in biomedical arena. Disadvantages include instability, fast excretion by the RES, limited sensitivity and cytotoxicity (Govender T et al., 1999; Zhang Z et al., 2006; Maeda H, 2001; Park JH et al., 2008).

A few superparamagnetic IO contrast agents were developed for MRI. These probes enable clearly defined anatomy imaging post contrast. Imaging molecular targets for early stage disease diagnosis requires probes with greater ability to amplify MRI signals (Weissleder R et al., 2001; Lee SJ et al., 2005). Besides IOs, another probe used for amplification strategy is quantum dots (QDs) as luminescence probes in fluorescence imaging.

2.10 Fluorescence Imaging

Fluorescence imaging is one of the major techniques in optical imaging. It is widely used in molecular biology and biochemistry laboratories. It can be applied in a large number of experimental, analytical and quality control applications. Besides probable side effects from the probes used, fluorescence imaging virtually has no other adverse effects and definitely does not involve radiation like most imaging techniques. Compared to other imaging modalities, fluorescent imaging modality has several important advantages including high sensitive detection, multicolor detection, probe

stability, low hazard and low cost (Liu Z et al., 2010). On the other hand, fluorescent imaging also has some disadvantages such as photobleaching, limited tissue penetrating depth, surface-weighted, relatively low spatial resolution and auto fluorescence disturbance (Liu Z et al., 2010). In view of these disadvantages, contrast agents such as organic fluorescent dyes and Quantum Dots (QDs) are often used to promote the fluorescence imaging.



Figure 2.10: IVIS Fluorescence imager.

(Adapted from <http://www.aomf.ca/xenogename.html>)

2.11 Fluorescence Imaging Principle

Fluorescence imaging works based on quantum theory. The contrast agents absorb a specific light frequency that is emitted from a proper imaging instrument to exactly raise their energy level to a brief excited state. Subsequently, these contrast agents

emit a fluorescent light whose wavelength is different from that of the absorbed light as they decay from this excited state as illustrated below. The imaging instrument detects this fluorescent light and based on the fluorescence signal from the whole sample, a fluorescent image is generated. The most often used fluorescent imaging instruments are wide field microscopes, confocal laser scanning microscopy, multi-photo microscopy, and deconvolution and 3D/4D image processors (Liu Z et al., 2010; Agarwal A et al., 2008).

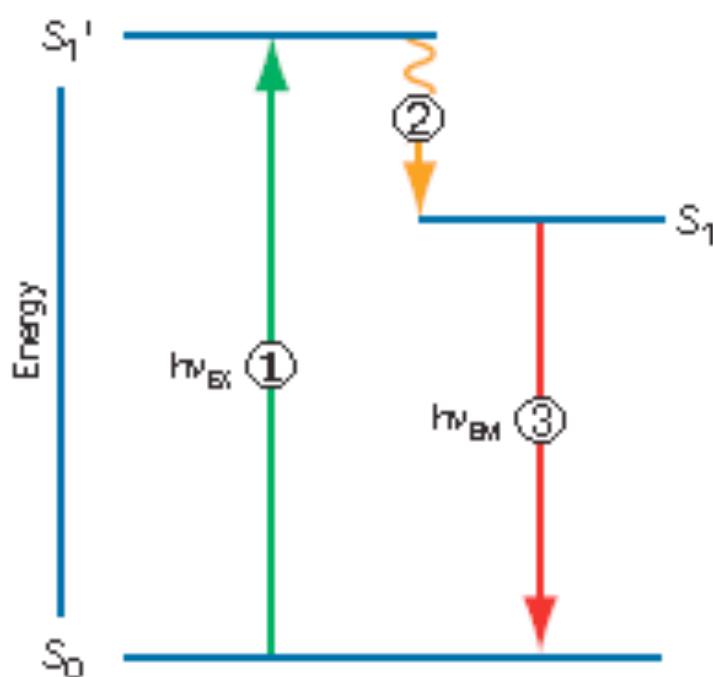


Figure 2.11: Jablonski diagram illustrating the processes involved in creating an excited electronic singlet state by optical absorption and subsequent emission of fluorescence. ①:Excitation; ②:Vibrational relaxation; ③:Emission.

(Adapted from <http://www.invitrogen.com/site/us/en/home/References/Molecular-Probes-The-Handbook/Introduction-to-Fluorescence-Techniques.html>)

2.12 Quantum Dots (QDs)

Quantum dots (QDs), also known as fluorescent semiconductor nanocrystals, are composed of atoms from groups II-VI or III-V of the periodic table. Cadmium selenide (CdSe), cadmium telluride (CdTe) and indium arsenide (InAs) are examples of fluorescent QDs that are most often used (Mishra B et al., 2010; Peng ZA et al., 2001). Various synthesis methods have been formulated to produce different forms of QDs. Such methods include colloidal synthesis, viral assembly, electrochemical assembly and bulk-manufacture. Among these, colloidal QDs, synthesized from colloidal synthesis, are most widely used.

QDs are predominantly spherical in shape with sizes ranging from 1 to 12 nm. They contain fluorophore, a molecule responsible for its luminescent properties. These luminescent properties are resulted from the quantum confinement effects. Upon irradiation, QDs absorb energy (at any wavelength greater than the energy of their lowest energy transition) and convert the energy into an extremely narrow bandwidth emission close to the band edge (Green M et al., 1999; Murray CB et al., 2000; Sutherland AJ, 2002).

2.13 Optical Properties of Quantum Dots (QDs)

Quantum dots are regarded to be the more superior fluorescent probes as compared to organic dyes (other fluorescent probes used popularly for bio-imaging). QDs have several outstanding optical advantages that make them excellent for biomedical applications. *In vivo* longevity is one major advantage of QDs, which enables extended applications *in vivo*, differentiating QDs from other fluorescent probes (Ballou B et al., 2004). Tunable emission from visible to infrared wavelength by changing the size and composition of QDs is another advantage of QDs. For instance,

CdSe QDs with a 2 nm diameter emit green light with a wavelength of 550 nm, whereas larger CdSe QDs with a 4 nm diameter emit lower energy red light with a wavelength of 630 nm (Sutherland AJ, 2002; Bruchez M et al., 1998). Apart from that, QDs also have broad excitation spectra with high absorption coefficients, high quantum yield of fluorescence, strong brightness, high resistance to photobleaching and good sensitivity (Pan J et al., 2008; Kim S et al., 2004; Gao XH et al., 2004).

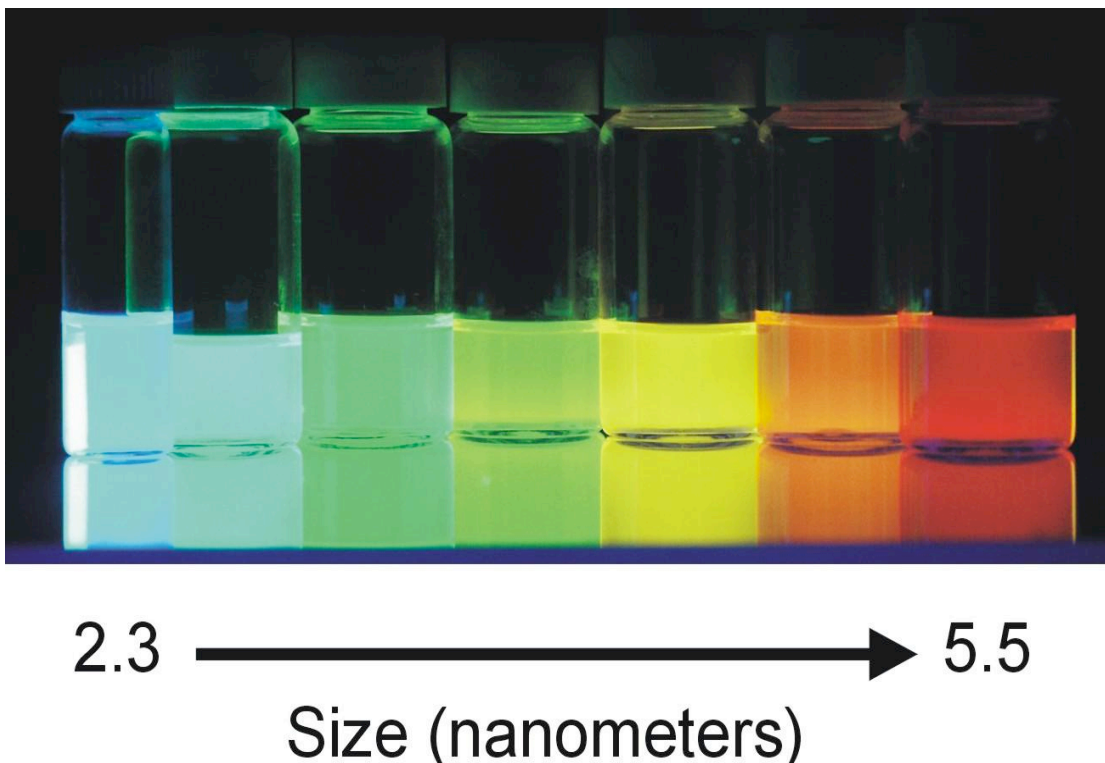


Figure 2.12: Excited quantum dots arranged according to size.

(Adapted from <http://www.elec-intro.com/quantum-dots>)

2.14 Applications of Quantum Dots (QDs)

As a result of the many optical advantages, QDs have been widely studied and utilized in many biomedical areas especially for bio-imaging. For instance, it is reported that QDs can be applied in fluorescent labeling for both *in vivo* cellular and

molecular imaging and *in vitro* assay detection. Besides that, QDs have also been used to trace cell line age, monitor physiological events in live cells, track cells *in vivo*, specifically mark cellular and molecular structures and measure cell mortality (Pan J et al., 2008). On top of that, QDs are also employed in DNA hybridization detection (Parak WJ et al., 2002). Luminescent colloidal semiconductor nanocrystals which contain CdSe-ZnS core-shell QDs are widely used for fluoroimmunoassay (Goldman ER et al., 2002) while QDs conjugated with internalin A and internalin B are used to detect food toxins (Gao XH et al., 2004). Various other applications of QDs are shown in the figure below:

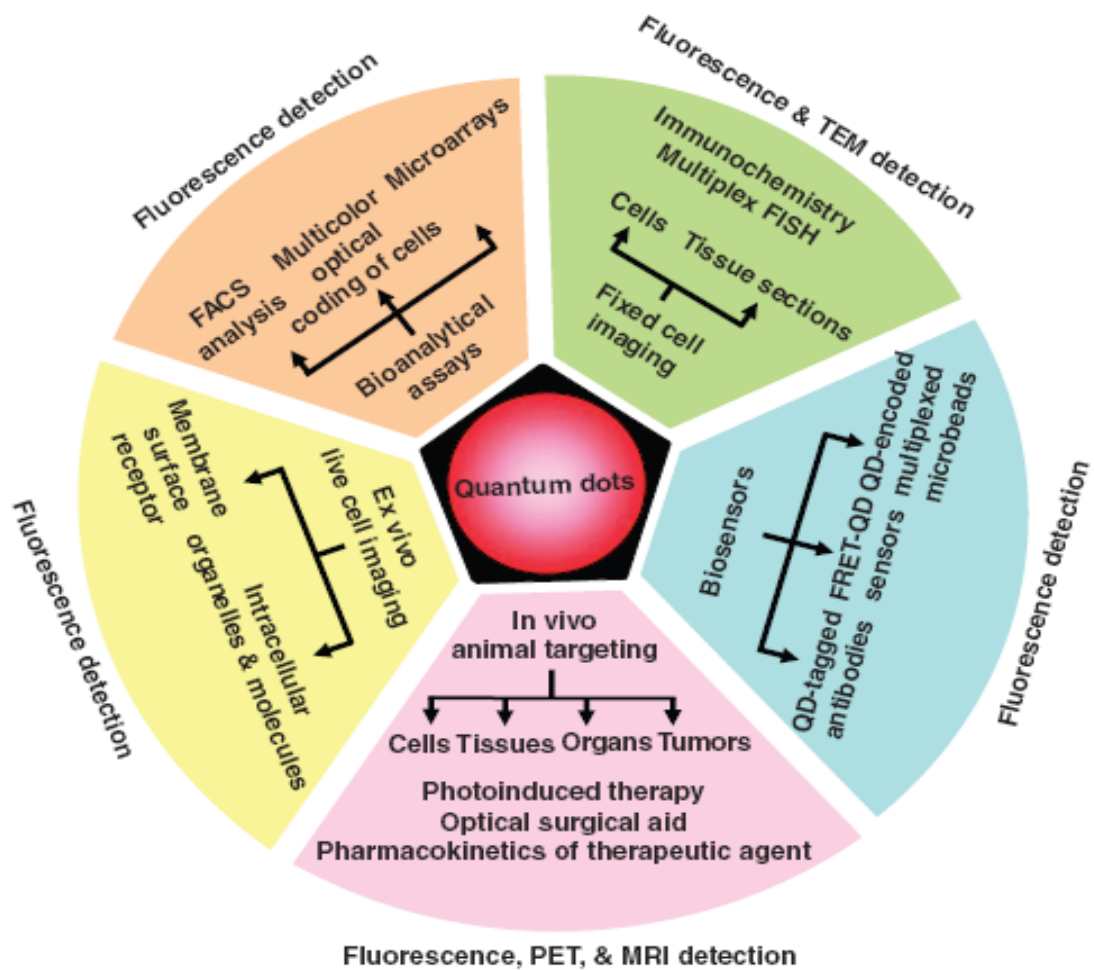


Figure 2.13: QDs applications (Michalet X et al., 2005).

2.15 Limitations of Quantum Dots (QDs)

QDs have been widely studied in many biomedical applications as a result of their various advantages. However, QDs usage does exist some limitations. One limitation is that the biocompatibility of QDs still remains rather unknown. The pharmacokinetic processes-absorption, distribution, metabolism and excretion (ADME) of QDs have not been explored nor understood. Generally, QDs may possibly have some toxic effects on the human body (Pan J et al., 2008). One report that led to this suspicion is a finding that reported CdSe/ZnS QDs to be toxic because of their release of Cd^{2+} ions. The Cd^{2+} ions are formed by surface oxidation of the QDs (Derfus AM et al., 2004). It is reported that CdSe QDs are highly toxic to cultured cells under UV illumination for prolonged periods. The CdSe QDs release toxic Cd^{2+} ions by photolysis under UV illumination as shown below:

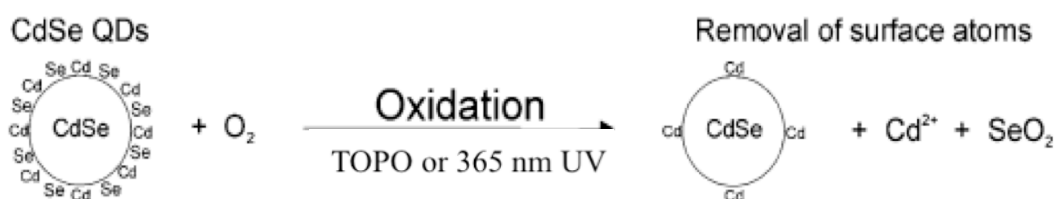


Figure 2.14: CdSe QDs release of toxic Cd^{2+} ions by photolysis under UV illumination (Derfus AM et al., 2004).

Besides toxicity related issues, another limitation of QDs is that their solubility in aqueous buffer is rather low. Normally, QDs are synthesized in hydrophobic organic solvents. Therefore, a layer of hydrophobic organic ligands is formed on their surface. As a result of this hydrophobic layer, QDs are insoluble in aqueous buffers and their

applications in the biological condition are therefore limited. Another limitation of QDs is that they have difficulties penetrating physiological drug barriers, resulting in low cell uptake efficiency. Last but not least, a major limitation is that QDs are fast excreted by the reticuloendothelial system (RES) (Pan J et al., 2008). This may result in QDs having short circulation time meaning that insufficient amount of the probe would find their way to the intended imaging site, resulting in poor imaging. QDs can be successfully applied in biology and medicine if these problems are solved.

2.16 Challenges of QDs and IO application in Imaging

2.16.1 Insufficient Probes at Imaging Site

Although necessary, amplification strategies are not enough to produce high quality images. Sufficient concentrations of probes must be gathered at the intended imaging area for an adequate period *in vivo*. Nevertheless, the agent dose is limited by the side effects of the agent itself and the rapid removal of probes from the blood system due to the body's mononuclear phagocyte system (MPS) interactions after opsonization (Puisieux F et al., 1994; Stolnik S et al., 1995).

2.16.1.1 Mononuclear Phagocyte System (MPS)

Although some probes may prove to be useful in binding to the targeted area of the body where imaging is intended in *in vitro* tests, they may have limited use due to their rapid removal from the blood system *in vivo*. This is due to interactions with the human body's mononuclear phagocyte system (MPS) (Puisieux F et al., 1994; Stolnik S et al., 1995) with the probes after opsonization. Phagocytes will attach to the opsonized foreign bodies when the attached opsonin proteins undergo conformational changes to form activated proteins detectable by phagocyte receptors (Donald E et al.,

2006). Non-specific attachment of phagocytes can also occur due to association of opsonin proteins on the hydrophobic foreign particle surface (Donald E et al., 2006; Frank M and Fries L, 1991). Complement activation, activated by one of several mechanisms including the classical, alternative and lectin pathway (Donald E et al., 2006; Puisieux F et al., 1994) also aids phagocyte attachment. Lastly, phagocytes engulf foreign particles by a process of endocytosis and commence secretion of enzymes and oxidative-reactive chemical factors such as superoxides and hydrogen peroxides to break down the particles (Donald E et al., 2006, Stolnik S et al., 1995).

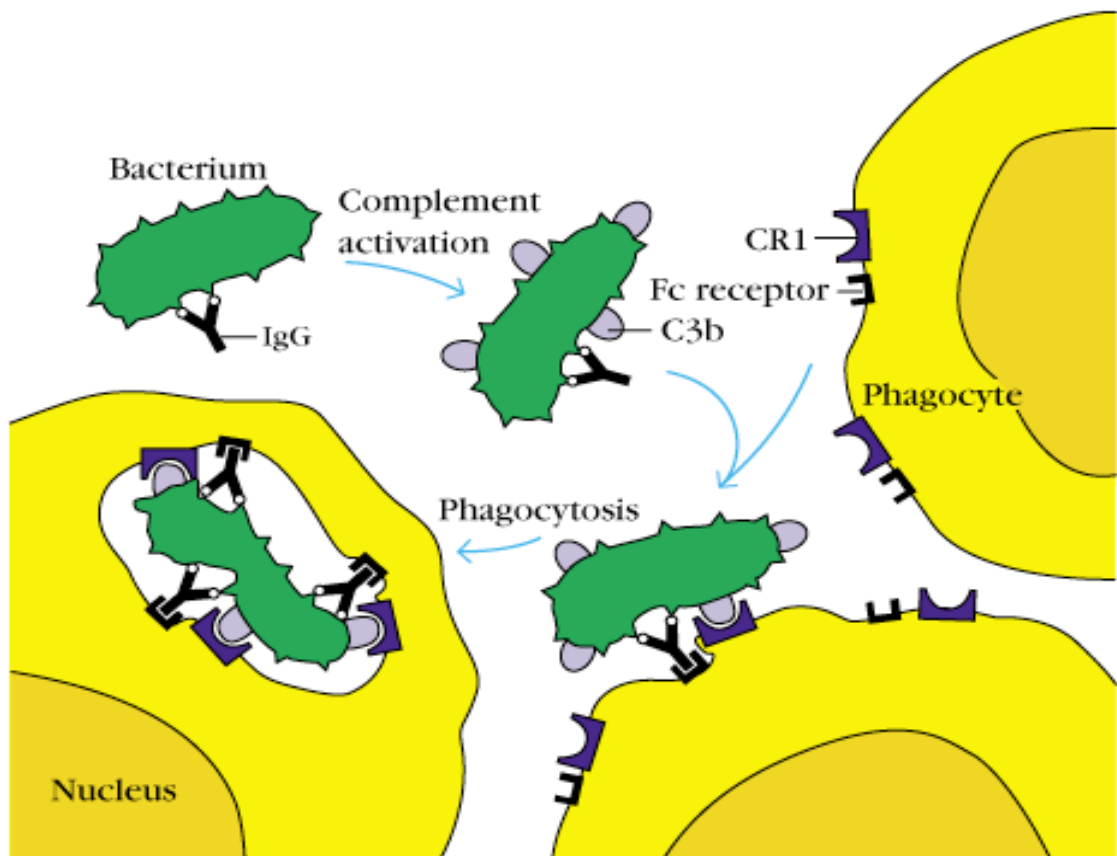


Figure 2.15: Opsonization and Phagocytosis of a bacteria.

(Adapted from <http://www.profelis.org/amc/vorlesungen/immunologie/komplement-system.html>)

2.16.1.2 Methods to Cloak Nanoparticles

Hence, it is evident that probes, which are not protected when injected into the body, can be swiftly removed by the MPS within a matter of seconds, rendering them ineffective (Gref R et al., 1994). Macrophages recognize probes as foreign entities due to the activated opsonin proteins, which are attached to the particles (Donald E et al., 2006). It is possible to devise methods to cloak nanoparticles and enable them to bypass MPS recognition, increasing their blood circulation half life (Illum L et al., 1984; Gref R et al., 1994; Kaul G et al., 2002). Methods to cloak nanoparticles from MPS recognition and therefore increase their half-life in circulation involve surface modification of the probes (Gref R et al., 1994; Illum L et al., 1984; Kaul G et al., 2002) to prevent opsonin proteins in the blood from being attached to the particles surfaces thus, escaping MPS detection.

Till now, there are no absolute solutions in completely preventing opsonization of particles. However, three decades of research has consolidated some trends and ways to hinder and slow down opsonization to increase circulatory time. Generally, hydrophilic particles opsonize slower than hydrophobic particles (Carstensen H et al., 1992; Muller RH et al., 1992; Norman ME et al., 1992) and neutrally charged particles opsonize slower than charged particles (Roser M et al., 1998). Therefore, non-charged, hydrophilic groups have been explored for grafting onto probes to hinder opsonization. These groups are usually long, flexible hydrophilic polymer groups and non-ionic surfactants that can shield hydrophobic and charged particles from opsonin proteins (Stolnik S et al., 1995).

Some proteins have been studied for their shielding properties and some have shown positive results. For example, chemically modified protein (bovine serum albumin) – coated QDs are stable for more than 2 years in buffer solution (Gao XH et al., 2002).

In addition to proteins, biodegradable polymers such as poly (lactic acid) (PLA) and poly(lactic-co-glycolic acid) (PLGA) and various biodegradable copolymers such as poly(lactic acid)-poly (ethylene glycol) (PLEA) copolymer and poly (lactide acid)-d- α -tocopheryl polyethylene glycol 1000 succinate (PLA-TPGS) copolymer have been used as shielding groups. One example of the use of shielding groups is this study in which polyethylene glycosylation was used to prolong the circulatory stability of recombinant human butyrylcholinesterase ([Chilukuri N et al., 2005](#)). The PEGylated particles were found to have an increased of circulation time from 18.3 h to 36.2 h in mice. Nanoparticle formulation using copolymers such as PLA-TPGS as encapsulating medium and shielding outer layer, can not only protect the particles from MPS, but also improve the water solubility of contrast agents such as QDs and IO. Encapsulation using PLA-TPGS for instance can improve the stability of QDs and IO and prolong the circulation lifetime of QDs and IO. On top of that, the nanoparticle formulation may improve the contrasting effect of QDs and IO compared to directly using commercial QDs and IO ([Wang Y et al., 2008](#)). As shown in the figure below, the IO-loaded biodegradable nanoparticles have better contrasting effect compared to commercial IO ([Wang Y et al., 2008](#)).



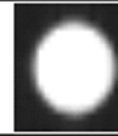

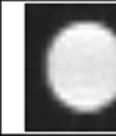
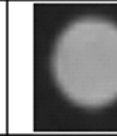

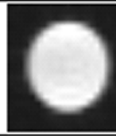

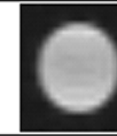
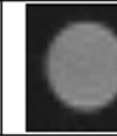
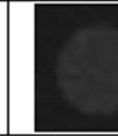
	Fe concentration (mM)					
	0	0.02	0.05	0.1	0.2	0.5
IOs						
NPs						

Figure 2.16: *In vitro* MRI of commercial IO (Resovist) and IO-loaded PLGA-mPEG nanoparticles suspended in water (TE=7 ms) (Wang Y et al., 2008).

In fact till date, the most effective and most commonly used polymers as shielding groups are the PEG and PEG-containing copolymers. Experimental research has visually demonstrated the shielding ability of PEGylated surfaces from opsonin protein attachment with the use of freeze fracture transmission electron microscopy (TEM) (Peracchia MT et al., 1999).

In summary, hydrophilic particles opsonize slower than hydrophobic particles (Carstensen H et al., 1992; Muller RH et al., 1992; Norman ME et al., 1992) and neutrally charged particles opsonize slower than charged particles (Roser M et al., 1998). Thus, non-charged, hydrophilic groups can be grafted onto the probes to hinder opsonization. These groups are usually long hydrophilic polymers and non-ionic surfactants, which can shield hydrophobic and charged particles from opsonin proteins (Stolnik S et al., 1995). To date, the most popularly used shielding groups are polyethylene glycol (PEG) and PEG-containing copolymers. One important example of such a copolymer is poly (lactic acid)-D-alpha-tocopheryl polyethylene glycol 1000 succinate (PLA-TPGS) that is gaining popularity in the research scene today.

2.16.2 Cytotoxicity

In addition, certain probes may have very good affinity with certain targets of imaging interest however they may pose to be toxic to the body. Hence, to make use of such probes, nanoparticle encapsulation by means of PEGylation may be needed as part of designing to reduce cytotoxicity of such probes. Derfus et al. demonstrated that the CdSe/ZnS quantum dots used as luminescence probes are highly toxic for the cells in culture as a result of the release of Cd²⁺ ions, caused by surface oxidation of quantum dots, and that the surface oxidation was repressed by coating with appropriate shells, decreasing the cytotoxicity of quantum dots. The reported surface coating work includes encapsulating quantum dots with dendrimer-like compounds, glass and amphiphilic polymers (Derkus AM et al., 2004). In 2005, Parak et al. extended the study of Derfus et al. and described that amphiphilic polymer-coated CdSe/ZnS nanocrystals in low concentrations could effectively prevent the release of Cd²⁺ ions from quantum dots surfaces, reducing their cytotoxicity (Kirchner C et al., 2003). In addition, more recently, Yan Wang et al., indicated in their paper that their iron oxide (IO) loaded PLGA-mPEG nanoparticle formulation achieves 36.9% and 35.6% less cytotoxicity after 48 h incubation at 20 and 50 µg mL⁻¹ Fe concentrations as compared to non-encapsulated IO particles of the same concentrations, respectively. Thus, reinstating the point that encapsulation with polymers reduces cytotoxicity (Wang Y et al., 2008).

The other method to decrease cytotoxicity is by targeted delivery. Targeting delivery of substances, in our case, contrast agents such as QDs or IO, can decrease their toxic effect on healthy cells. Targeting can be divided into passive targeting and active targeting (Pan J et al., 2008).

2.16.2.1 Tumor Targeting

The ability of the nanoparticles to reach the intended tissues/tumors is vital both in diagnostic imaging and drug delivery. Non-specificity of the nanoparticles can cause them to bind to healthy tissues and risk damaging them. To limit non-specific binding, nanoparticles can be modified to increase its affinity for the target tissues. This can be done in two ways: passive and active targeting.

2.16.2.2 Active Targeting

Cancer cells often over express either proteins that are usually found at low levels on healthy cells (tumor-associated antigens) or proteins that can be found only on cancer cells (tumor-specific antigens). Active targeting works by attaching ligands to a targeting component that binds with antigens expressed on the target tissue. This would direct the drugs or contrast agents towards the targeted organ, tissue or cells and cause them to accumulate at these sites. Active targeting allows the drugs/contrast agents to be delivered to the intended site, which reduces the side effects as well as promotes cellular uptake of these loadings by receptor-mediated endocytosis. Receptor-mediated endocytosis is the process whereby the ligands bind to the receptors on the cell surface followed by internalization through coated pits and vesicles into the cells ([Park JH et al., 2008](#)).

2.16.2.3 Passive Targeting

In passive targeting, the nanoparticles (QDs and IO loaded PLA-TPGS in our case) accumulate at the tumor through the enhanced permeability and retention (EPR) effect. Tumor blood vessels differ from normal blood vessels in which there are a relatively high proportion of fast growing endothelial cells, increased irregularity,

pericyte deficiency and abnormal basement membrane formation. Cancer cells require lots of oxygen and nutrients for their rapid growth. This in turn stimulates fast production of blood vessels. Vascular structures resulted from rapid growth, are defective and lack effective lymphatic drainage system, rendering the vessels permeable to macromolecules and small particles. Because of the lack of efficient lymphatic drainage, these particles cannot be cleared effectively and hence accumulate in the tumor. This effect is known as the enhanced permeability and retention effect (Maeda H, 2001). As our hypothesized probe system does not include active targeting ligands, passive targeting is the prime objective for our probe system to achieve.

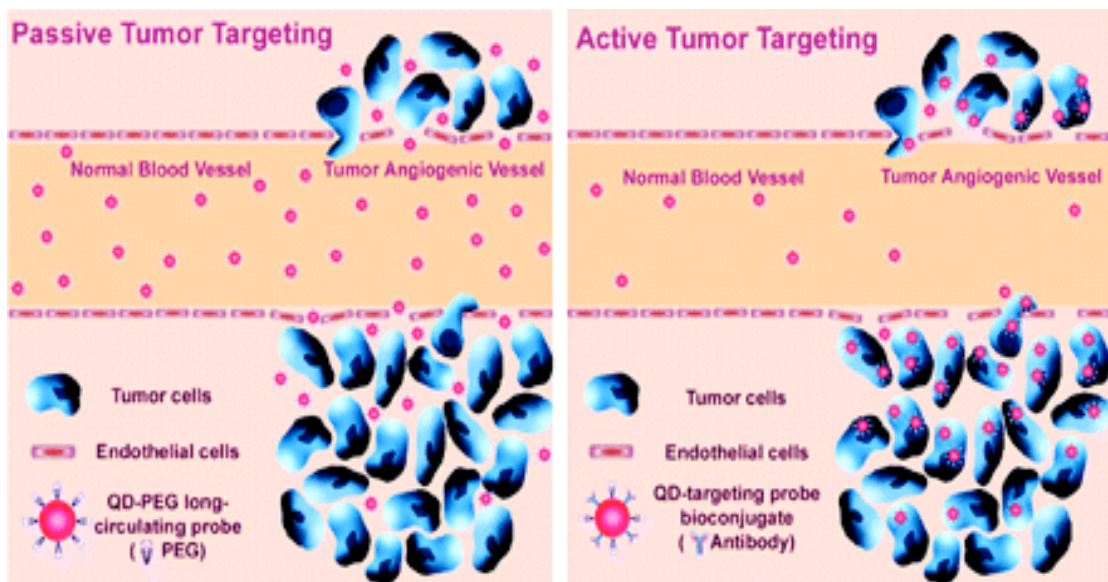


Figure 2.17: Passive and active tumor targeting.

(Adapted from <http://www.ajnr.org/cgi/content/full/30/7/1293/F2>)

2.17 Nanotechnology in Molecular Imaging

As mentioned earlier, the first factor for molecular imaging to be possible is the presence of high affinity probes with reasonable pharmacodynamics. Such probes used are usually nanoparticles. Nanoparticles are basically particles sized between 1 and 100 nanometers. Their size limitation can be restricted to two dimensions and they may or may not exhibit size-related properties that differ significantly from those observed in fine particles or bulk materials.

The nanoparticle probes used for molecular imaging can be small molecules such as receptor ligands or bigger higher molecular weight affinity ligands such as recombinant proteins. The advantage of synthesizing imaging probes into nanoparticles is that the probes when reduced to such a small scale will not only be able to escape MPS detection (increasing circulation time) but also have a higher probability of being uptaken by cells.

Advances in drug discovery technology today have made the discovery of potential affinity ligands very effective and efficient against the thousands of targets where imaging may be of interest. Further design and refining efforts are made on these potential ligands before they can be used as probes for molecular imaging.

As discussed earlier, certain probes may have good affinity with certain targets of imaging interest but pose to be toxic. An example is QDs, which are made up of elements that are toxic in individual elemental form. An appropriate modification and formulation of QDs could minimize their toxicity (Gao XH et al., 2005; Wang X et al., 2008). Formulation of imaging probes such as IOs and QDs in nanoparticles of biodegradable polymers may thus provide an ideal solution as well as enhance cellular uptake, hence improving imaging effects (Wang Y et al., 2008). Moreover, the imaging agent-loaded nanoparticles can be further conjugated with biological

ligand to realize targeted delivery of the imaging agent to the diseased cells, which can be distinguished from healthy ones. The nanoparticles surface decorated with targeting ligand enables the selective delivery of imaging agent into diseased cells by the ligand-mediated approach, which achieves high specificity and sensitivity of cancer detections, allowing the diagnosis of cancer at its earliest stage.

2.18 Multi-modality

IO and QD probes are effective probes for amplification in molecular imaging. However, individual imaging probes have their advantages and disadvantages. No single imaging modality is perfect to satisfy all the requirements for bio-imaging. For instance, IO probes provide high spatial resolution and unlimited depth penetration (Medarova Z et al., 2006) but their sensitivity in imaging fails in comparison to optical fluorescence imaging probes such as QDs. QDs, in turn; have excellent imaging effects and long half-life, but their ability for tissue penetration is limited due to the refraction and adsorption of light in the living organism. Therefore, it is very important to find an imaging method that can fulfill the requirements in medical applications as much as possible, and this can be achieved by applying multi-modal imaging.

Multi-modal imaging means applying two or three or even more imaging modalities concurrently. Multimodal imaging can be developed to make use of the advantages and overcome the limitations, which can be realized by co-encapsulation of QDs and IOs in ligand-conjugated nanoparticles of biodegradable polymers.

There have been some studies involving remodelling imaging probes suited for dual modality imaging capabilities. Xie J et al. encapsulated dopamine modified IO nanoparticles into HAS matrices which permit applications in MRI. Such HAS-IO

nanoparticles were labelled with Cy5.5 dye and ^{64}Cu -DOTA chelates which permits applications in NIRF imaging and PET imaging respectively (Xie J et al., 2010).

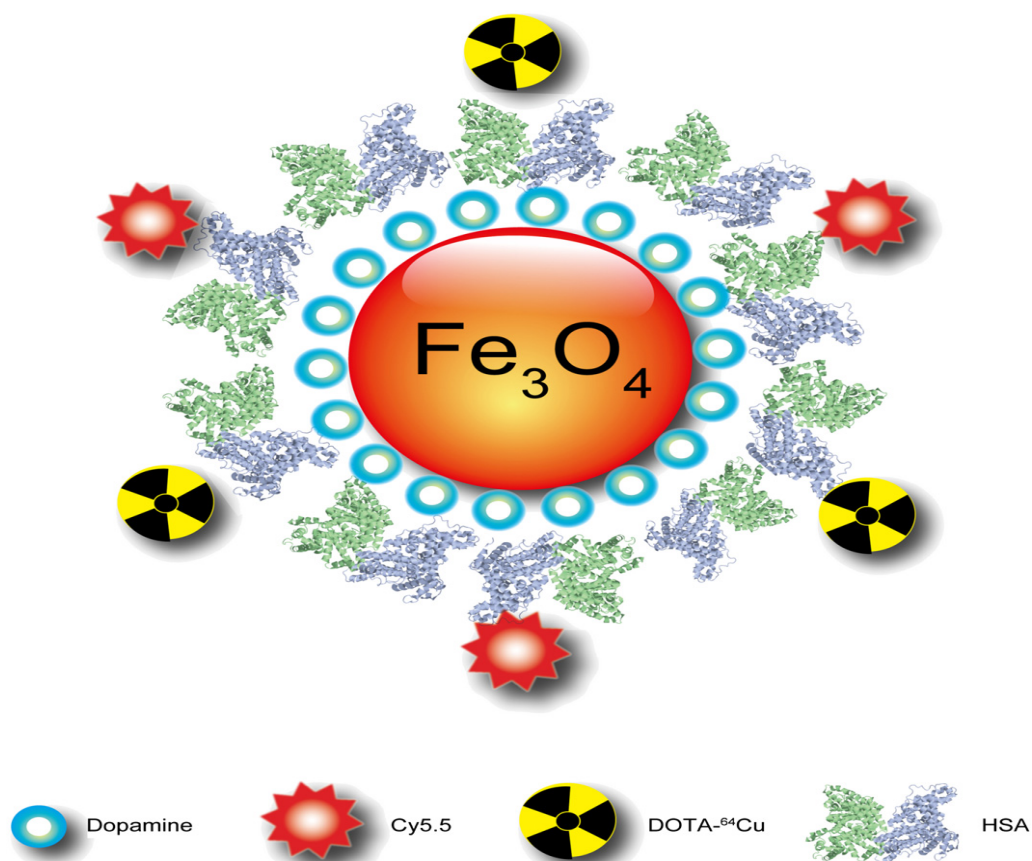


Figure 2.18: Schematic illustration of the multi-functional HSA-IONPs. The pyrolysis-derived IONPs were incubated with dopamine, after which the particles became moderately hydrophilic and could be doped into HSA matrices in a way similar to drug loading (Xie J et al., 2010).

In this triple modality system, MRI offers a high spatial resolution. However, MRI has the issue of limited sensitivity. Therefore, PET and NIRF were utilized to compensate for this drawback. Between these two, PET provides a better signal-to-noise ratio. NIRF, on the other hand, can be visualized both *in vivo* by an IVIS system

and *ex vivo* by fluorescence microscopy, playing a unique role of bridging the *in vivo* and histological observations.

In another study by Zhou et al., the concept of upconversion luminescence (UCL) and MR dual-modality imaging *in vivo* of whole-body animals was explored. In the work, $\text{Tm}^{3+}/\text{Er}^{3+}/\text{Yb}^{3+}$ co-doped NaGdF_4 was synthesized with near-infrared to near-infrared upconversion luminescent and magnetic resonance properties (Zhou J et al., 2010). Also, Choi *et al.* explored hetero-structured complexes formed by magnetic iron oxide nanoparticles and near-infrared (NIR) fluorescent single-walled carbon nano-tubes (SWNT) (Choi JH et al., 2007). These complexes, when further conjugated with monoclonal antibodies to target specific receptor site, could be used to provide molecular-level contrast and bio-sensing.

In another multi-modal study, Rieter, WJ et al. found that hybrid silica nanoparticles could also be used as multi-modal contrast agents for *in vitro* optical and T1-and T2-weighted MRI (Rieter WJ et al., 2007). Each hybrid silica nanoparticle contains a luminescent $[\text{Ru}(\text{bpy})_3]\text{Cl}_2$ core (bpy=2,2'-bipyridine) and a paramagnetic monolayer or multilayer coating of a silylated Gd complex. The luminescent core acts as a contrast agent for optical imaging and Gd^{3+} (containing microemulsions) acts as a T₁ contrast agent. The optical imaging has high sensitivity while MRI has high spatial resolution. The dual modalities system can have high sensitivity as well as high spatial resolution.

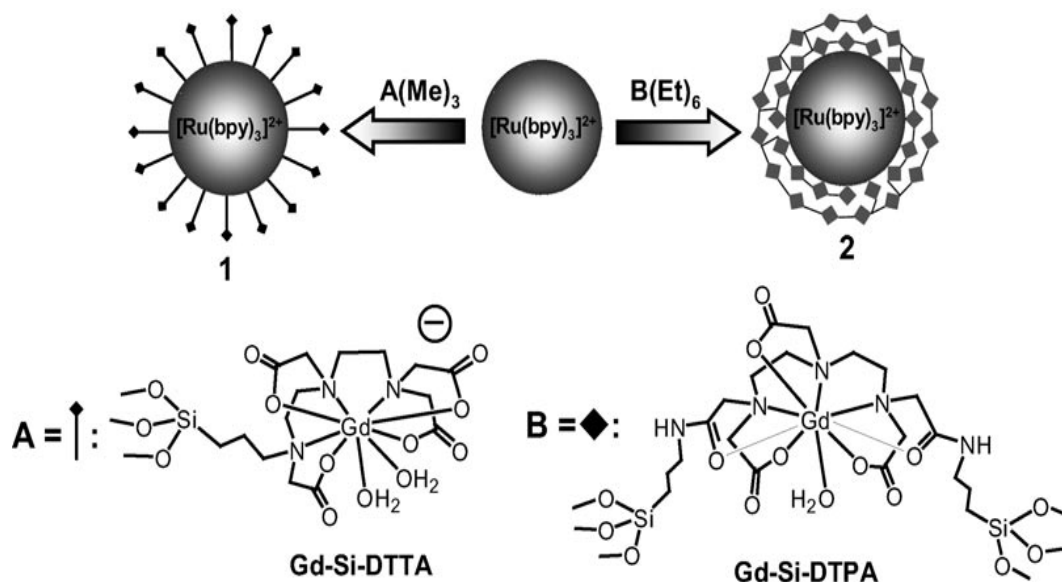


Figure 2.19: Synthesis of hybrid silica nanoparticles (Rieter WJ et al., 2007).

Hwang DW et al also developed a nucleolin-targeted multimodal nanoparticle-imaging probe for tracking cancer cells using an aptamer. This multimodal nanoparticle-imaging probe can be used in fluorescence imaging, radionuclide imaging and MRI *in vivo* concurrently (Hwang DW et al., 2010). ^{67}Ga -MNP@SiO₂(RITC)-PEG/NH₂-AS1411 (MFR -AS1411) nanoparticles are made up of magnetic cobalt ferrite in the central core and rhodamine B isothiocyanate fluorescence dye (MF) coated with a silica shell. In addition, polyethylene glycol (PEG), Fmoc-protected amine moieties, and a carboxyl group surround the surface of the particles, which were further labeled with AS1411 aptamer, *p*-SCN-bn-NOTA chelator and ^{67}Ga -citrate.

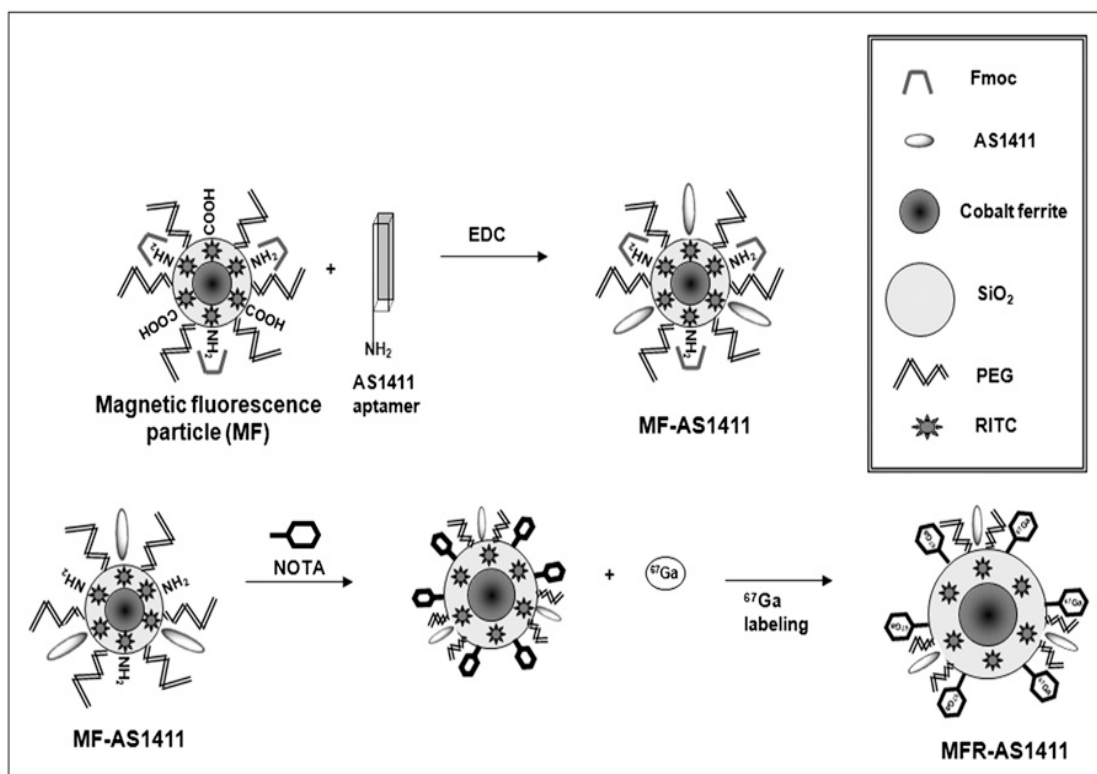


Figure 2.20: Schematic illustration of MFR-AS1411 synthesis. MF particles had carboxyl group and Fmoc-protected amine moiety, which was coupled with amine terminated AS1411 aptamer using EDC (MF-AS1411). After reaction of MFAS1411 with p-SCN-bn-NOTA, particles were reacted with ⁶⁷Ga-citrate to form MFR-AS1411 (Hwang DW et al., 2010).

The magnetic cobalt ferrite is the contrast agent for MRI. MF is the contrast agent for fluorescence imaging and ⁶⁷Ga-citrate is the contrast agent for radionuclide imaging. This multi-modal imaging system offers a broad range of imaging possibilities, ranging from *in vitro* cellular studies using fluorescence materials to bioluminescence imaging in animal models and radionuclide and MRI for potential diagnostic and therapeutic human application (Hwang DW et al., 2010).

To achieve a thorough analysis of one multi-modal imaging system, *in vivo*, *ex vivo* and *in vitro* analyses should be done and cross-referenced. Most of the studies listed

above, however, are related either to *ex vivo* or *in vitro* analysis. Most of them were lacking in *in vivo* analysis. Furthermore, some of the studies lack clinical feasibility as they involve the use of probes for imagers, which are either not available or impractical in the current medical scene. In addition, some imaging modalities such as CT and radionuclide imaging explored have significant side effects on human health.

As mentioned before, both fluorescence imaging and MRI are non-invasive and will not cause radiation injury. On top of that, the QDs and IO as contrast agents for fluorescence imaging and MRI respectively have been widely studied in biomedical applications. Therefore, encapsulation both QDs and IO in PLA-TPGS copolymers as multi-modal imaging probes should provide high quality images. This multi-modal imaging probe should have high sensitivity and depth penetration.

In this study, IO contrast agent and fluorescence QDs are co-encapsulated in a biodegradable polymer, poly(lactide)—tocopheryl polyethylene glycol succinate (PLA-TPGS), which was a new type of biodegradable copolymer synthesized in our laboratory (Zhang Z et al., 2006). PLA provides the needed mechanical strength and enough biodegradability for extended blood circulation times, while TPGS component reduces cytotoxicity and provides stealth from RES as well as enhances chemotherapy by inhibiting P-gp activity, i.e. the multiple drug resistance (MDR) effects (Dintaman JM et al., 1999; Johnson BM et al., 2002). The IOs and QDs were encapsulated in the polymer matrix of PLA-TPGS by a modified nanoprecipitation technique. Particle characterization was performed and the probe was tested *in vitro* for cytotoxicity and cell uptake. Furthermore, the multimodal probe was tested *in vivo* on tumor xenograft grown on immune deficient mice. This multimodal probe enabled tumor visualization for both MRI and fluorescent imaging. The results showed that the multimodal probe could provide an enhanced avenue for a more detailed imaging

procedure, reducing the possibility of overlooking any inherent problem which may have been the result of poor imaging due to limitations of using a single modality probe.

CHAPTER 3: MATERIALS & METHODS

3.1 Materials

Organic Quantum Dots (Qdot®655 ITK™; catalog number Q21721MP) and Carboxyl Quantum Dots (Qdot®655 ITK™; catalog number Q21321MP) were purchased from Invitrogen Corporation Singapore. Iron Oxide (IO) dispersed in THF is prepared from Resovist® provided by a colleague from another laboratory. Tetrahydrofuran (THF), Penicillin-streptomycin solution and trypsin–EDTA solution were provided by Sigma–Aldrich (Sigma–Aldrich Pte Ltd, Singapore). Fetal bovine serum (FBS) was purchased from Gibco (Life Technologies AG, Switzerland). DMEM medium was from Invitrogen Corporation. All chemicals used in this study were HPLC grade. Millipore water was produced by the Milli-Q Plus System (Millipore Corporation, Bedford, USA). MCF-7 breast cancer cells were provided by American Type Culture Collection. PLA-TPGS copolymer was synthesized according to a method described in our previous work ([Zhang Z et al., 2006](#); [Prashant C et al., 2010](#)). The PLA:TPGS component ratio for the PLA-TPGS copolymer used in this research is 90:10 w/w. Nuclear magnetic resonance spectroscopy (NMR) testing on the copolymer revealed that the copolymer synthesized has number-averaged molecular weight (Mn) of 17,027.

3.2 Synthesis Methods

3.2.1 Flocculation of QDs

The Organic QDs from Invitrogen were dispersed in n-decane. To prepare the QDs in THF, 1200 μL of alcohol mixture (75% methanol: 25% propanol) was added to 200 μL of organic QDs (equivalent of 0.23 mg Cd as determined by ICP-MS). The solution was then vortexed for 2 minutes and subjected to centrifuging for 15 minutes at 11,000 rpm. The supernatant was removed and 1 mL of THF was added to disperse the QDs.

3.2.2 Formulation of QDs and IOs-loaded NPs

The QDs and IOs-loaded NPs were prepared by a modified nanoprecipitation method ([Prashant C et al., 2010](#)). The previously flocculated QDs were dispersed in 1 mL THF (equivalent of 0.23 mg Cd as determined by ICP-MS), 20 μL of IOs solution in THF (containing 1 mg of IO) and 100 mg of PLA-TPGS copolymer were dissolved in 5 mL THF. The resulting solution was poured gradually into 30 mL of aqueous phase containing 15% (w/v) TPGS as emulsifier. The mixture was then sonicated at 25 W output until homogeneity was achieved and then diluted with water to aid diffusion of the organic solvent and precipitation of the nanosized particles. The resultant solution was stirred continuously overnight to allow the organic solvent (THF) to vapourize. The particle suspension was centrifuged at 10,500 rpm for 15 min to obtain the NPs in the pellet. The NPs were washed thrice with deionized (DI) water and subsequently freeze-dried. The dried particles were diluted with MilliQ water or PBS whenever required.

3.3 Characterization of QDs and IOs-loaded NPs:

3.3.1 Particle Size and Size Distribution

The average particle size and size distribution of the QDs and IOs-loaded PLA-TPGS NPs were measured using laser light scattering (LLS, 90 Plus Particle Size, Brookhaven Instruments Co., USA). The NPs were diluted with DI water and sonicated for 2 minutes before measurement.

3.3.2 Surface Charge

The zeta potential of the QDs and IOs-loaded PLA-TPGS NPs was determined with ZetaPlus zeta potential analyzer (Brookhaven Instruments Corporation) at room temperature. The samples were diluted with DI water before measurement. Six measurements were taken and the average was recorded.

3.3.3 TEM Analysis

The shape of the PLA-TPGS NPs and the encapsulation of the IOs and QDs were verified by transmission electron microscope (TEM, JEM-2010F, JEOL, Japan). For the preparation of TEM samples, drops of diluted NPs were added onto the surfaces of formvar-coated copper grids. The NPs were left to dry at room temperature.

3.3.4 QDs and IOs Encapsulation Efficiency

The encapsulation efficiencies of QDs and IO in the PLA-TPGS NPs were evaluated using the inductively coupled plasma mass spectrophotometer (ICP-MS, Model: Agilent Technologies 7500 series G3271A). A known amount of the QDs and IOs-loaded PLA-TPGS NPs was dissolved in 1 mL of reagent grade 65% nitric acid and boiled for 2 h at 80 °C. The resultant solution was then diluted with MilliQ water to

the desired volume for ICP-MS analysis to determine the actual amount of the Cadmium (from QDs) and Fe (from IOs) encapsulated in the NPs. The dosages of QDs and IOs were also prepared separately in the same way for ICP-MS analysis to determine the actual amount of individual Cd (from QDs) and Fe (from IO) added during particle synthesis. The intensities obtained were compared to that of the Cd and Fe standards for quantization (Sigma-Aldrich, Singapore). The percentage QDs and IOs encapsulation efficiencies were obtained in comparison with the amount dosed.

3.3.5 XPS

To confirm that the IO and QDs detected from the synthesized nanoparticles were encapsulated within the nanoparticles and not merely on the surfaces of the particles, the particles are sent for X-ray photoelectron spectroscopy (XPS) testing. X-ray photoelectron spectroscopy (XPS) can be applied to determine the elements or components presented on the surface of a compound within a depth range of 1 to 10 nm. The samples are prepared simply by dropping a small drop of the samples on a piece of glass chip. The sample particles were also crushed to release the IO and QDs within and tested using XPS again to act as control.

3.4 Cell Line Experiment

3.4.1 Cell Cultures

The MCF-7 breast cancer cells used in the cell studies were cultured using DMEM medium supplemented with 10% FBS and 1% antibiotics. The cells were cultivated at 37 °C in humidified environment of 5% CO₂. The cells were pre-cultured until confluence was reached before they were used for *in vitro* studies (Win KY et al., 2005).

3.4.2 *In vitro* cellular uptake of NPs

For qualitative study, MCF-7 cells were cultivated in the chambered cover glass system (LAB-TEK®, Nalgel Nunc International, Rochester, NY) with 5% CO₂ in DMEM at 37 °C as proposed by American Type Culture Collection. After 24 h incubation time, the adherent cells were washed twice with PBS and 50 µL of QDs and IO-loaded NPs (diluted to have the NPs of QDs equivalent to 1 µg Cd in 1 mL of media) were added into the chambers. The cells were incubated with the NPs for 4 h and were washed 4 times with PBS after incubation. They were then fixed by 70% ethanol for 15 minutes. The cells were washed twice again with PBS and the nuclei were stained with 4,6-Diamidino-2-phenylindole dihydrochloride (DAPI) for 30 minutes. Following this, the cells were washed twice with PBS and observed using the confocal laser-scanning microscope (CLSM, Olympus Fluoview FV1000, Japan). For quantitative study, MCF-7 cancer cells were incubated in 96-well black walled plates (Nunc, Roskilde, Denmark) with the cell density in the range of 40,000 – 50,000 cells/mL. After 24 h, the old medium of the sample wells was discarded and the cells were incubated for 1, 2 and 4 h respectively in 100 µL of QDs and IO-loaded

NPs of concentrations containing 1 $\mu\text{g/mL}$ Cd, 0.5 $\mu\text{g/mL}$ Cd and 0.25 $\mu\text{g/mL}$ Cd dispersed in the medium. Wells of cells used as the control had their old medium removed and topped up with 100 μL of QDs and IO-loaded PLA-TPGS NPs of the respective QD concentrations dispersed in PBS. After 1, 2 and 4 h respectively, the sample wells were washed thrice with PBS and finally filled with 100 μL of PBS. 50 μL of 0.5% triton X-100 in 0.2 N NaOH was added to all the wells. The fluorescence intensities of the cells were measured using the microplate reader (Genios, Tecan, Männedorf, Switzerland). The excitation wavelength was set at 530 nm and emission wavelength at 652 nm. The cell uptake was calculated using the formula below:

$$\text{Cell Uptake (\%)} = (\text{InS} / \text{InC}) \times 100 \quad (3.1)$$

where InS is the fluorescence intensity of the cells in the sample wells and InC is the fluorescence intensity of the cells in the wells acting as controls.

3.4.3 *In vitro* Cytotoxicity

MCF-7 cancer cells were incubated in 96-well black walled plates (Nunc, Roskilde, Denmark) with the cell density in the range of 40,000 – 50,000 cells/mL. After 24 h, the old medium was discarded and the cells were incubated for 24 or 48-h intervals. In each case, the cells were treated in the free QDs (containing 1.42 $\mu\text{g/mL}$ Cd); free IO (containing 5.73 $\mu\text{g/mL}$ Fe) or the QDs and IOs-loaded PLA-TPGS NPs (containing 1.42 $\mu\text{g/mL}$ Cd and 5.73 $\mu\text{g/mL}$ Fe) dispersed in the medium. At the 24 h and 48 h intervals, the cultured cells were assayed for cell viability with methylthiazolyldiphenyl-tetrazolium bromide (MTT, Sigma). The wells were washed twice using PBS and then 10 μL of MTT supplemented with 90 μL culture medium was added into each well. After 24 h or 48 h incubation in the incubator, the culture medium was removed and the purple crystals were dissolved in DMSO. The

fluorescence intensities of the cells were measured using the microplate reader (Genios, Tecan, Männedorf, Switzerland). The absorbance wavelength was set at 570 nm and background wavelength at 660 nm. Cell viability was calculated in comparison with that of the control (consisting of the untreated cells).

3.5 Animal Study

The animal protocol was approved by the Institutional Animal Care and Use Committee (IACUC), National University of Singapore (#802/05(A10)09).

Xenograft model was developed using SCID mice (female, 20 g). MCF-7 cancer cells were injected into the subcutaneous layer of the mice near the right flank at a concentration of 10^6 cells (100 μ l). The tumors were allowed to develop to volumes of 150-200 mm³.

3.5.1 Tumor imaging (MRI)

MRI was performed on the mice on a Bruker 7T Clinscan MRI system and was approved by the A*STAR Institutional Animal Care and Use Committee. Contrast agent was injected (dosage: 6.0 mg of Fe/kg body weight or equivalent of 1.5 mg of Cd/kg of body weight) through tail veins of the mice under 1% isoflurane anesthesia. T₂-weighted images were acquired at various time points using T₂-weighted turbo spin-echo sequence (TR/TE=1500/36 ms, resolution=100 μ m, thickness=1 mm). MRicro 1.40 (Chris Rorden ©1999-2005) was used to analyze the region of interest (ROI) of the MRI images. The images were color coded and the color was compared with that of the scale of signal intensity provided. Higher intensity was at regions of white and lower intensity at regions of black.

3.5.2 Tumor Imaging (Fluorescent Imaging)

For fluorescent imaging study, the mice were sorted into 2 groups of 4. The mice in one group received a dose of the QDs and IO-loaded PLA-TPGS nanoparticles. Each 20 g mouse was injected with the NPs formulation (dosage: 1.5 mg of Cd/kg of body weight or equivalent of 6.0 mg of Fe/kg body weight). The mice in the other group were left without any treatment to act as control. After 6 hours, perfusion procedures were conducted on all the mice to cleanse their organs of blood using PBS and fix them with formaldehyde. During perfusion, the anaesthetized mice had PBS introduced into them first via the left ventricles of their hearts to cleanse their organs. The superior and inferior vena cavae were snipped to release blood from the mice. 4% formalin was then introduced via the left ventricles to fix the organs. The organs were then harvested and used for fluorescent imaging. To monitor red fluorescence signals of QDs, *ex vivo* red fluorescence imaging of organs was acquired by IVIS imaging system (IVIS 100) coupled with cool CCD camera (Xenogen, Alameda, CA, USA). The detected light emitted from QDs was digitized and electronically displayed as a pseudo colour overlay onto a grayscale image of the organ. Images and measurements of fluorescence signals were acquired and analyzed with the Xenogen living imaging software v2.5 and quantified as photons per second. The acquired signal intensities were displayed as a percentage increase after being compared to the controls used in the experiment.

3.5.3 Biodistribution

For biodistribution study, the mice were sorted into 2 groups of 4. The mice in one group received a dose of QDs and IOs-loaded PLA-TPGS nanoparticles. Each 20 g mouse was injected with the NPs formulation (dosage: 6.0 mg of Fe/kg body weight or equivalent of 1.5 mg of Cd/kg of body weight). The mice in the other group were left without any treatment to act as control. After 6 hours, perfusion procedures were conducted on all the mice to cleanse their organs of blood using PBS and fix them with formaldehyde. The mice were then sacrificed and their organs were collected, cryo-sectioned using a cryostat (LEICA CM3050S) and examined using the confocal laser-scanning microscope (CLSM, Olympus Fluoview FV1000, Japan).

CHAPTER 4: RESULTS & DISCUSSIONS

4.1 Characterization of QDs and IOs-loaded nanoparticles

4.1.1 Size and Size Distribution

The size and size distribution of the QDs and IOs-loaded PLA-TPGS nanoparticles were measured by laser light scattering (LLS, 90-PLUS Analyzer, Brookhaven Instruments Corporation, USA) and are shown in Table 3.1. It can be observed that the diameters of the nanoparticles were around 325.8 nm with a PDI of 0.204. This shows that the particles were quite uniform in size and within the optimum cellular uptake range.

4.1.2 Surface Charge

The QDs and IOs-loaded PLA-TPGS nanoparticles were negatively charged at about -37.3 mV as shown in Table 3.1. Zeta potential is an indicator of the stability of the nanoparticle suspension. A higher electric charge on the surface of the nanoparticles will prevent aggregation of the nanoparticles in buffer solution because of the strong repellent forces among particles (Mu L et al., 2002). Therefore, the nanoparticles synthesized in this study were stable in solution.

Nanoparticle	Size (nm)	PDI	ZP (mV)	EE %	
				Fe 54	Cd 111
QDs & IOs-loaded PLA-TPGS NPs	325.8 ± 5.2	0.204 ± 0.065	- 37.3 ± 5.10	60.00 ± 14.14	45.00 ± 7.07

Table 4.1: Characteristics of the QDs and IOs-loaded PLA-TPGS nanoparticles including particle size and polydispersity (PDI), zeta potential (ZP) and encapsulation efficiency percentage (EE%).

4.1.3 TEM Analysis

From the TEM image of QDs and IOs-loaded PLA-TPGS nanoparticles in Figure 4.1C, well-formed nanoparticle with dark spots (QDs and IOs) encapsulated can be clearly seen. The QDs and IOs were encapsulated uniformly in the polymeric nanoparticle. As comparison, Figure 4.1A shows a TEM image of the IOs-loaded PLA-TPGS nanoparticles and Figure 4.1B shows that of the QDs-loaded PLA-TPGS nanoparticles. It can be observed that the QDs were actually elliptically shaped while the IOs were more spherically shaped. These TEM images show that the PLA-TPGS NPs were spherically shaped.

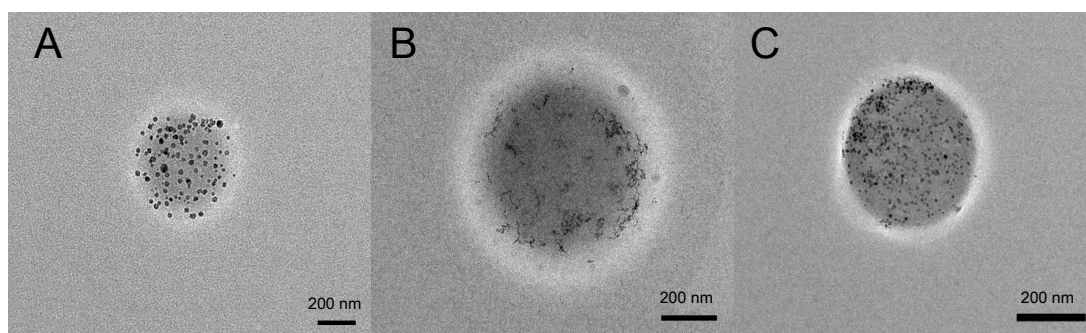


Figure 4.1: TEM Images of A: the IOs-loaded PLA-TPGS NPs, B: the QDs-loaded PLA-TPGS NPs and C: the QDs and IOs-loaded PLA-TPGS NPs (scale bar = 200 nm).

4.1.4 QDs and IO Encapsulation Efficiency

It is difficult to differentiate the QDs from the IOs in the PLA-TPGS nanoparticles solely based on the TEM images. Hence, it is important to make use of the ICP-MS to measure the amount of Cd and Fe contents present in the PLA-TPGS nanoparticles to quantify the amount of the QDs and IO inside. The QDs and IOs encapsulation efficiencies in the PLA-TPGS nanoparticles are demonstrated in Table 4.1. The encapsulation efficiency of QDs is about 45% while that of IOs is about 60%. In general, the encapsulation efficiencies of QDs and IOs are relatively high. This may be due to the use of TPGS as the emulsifier at a relatively high concentration (15% by weight). TPGS is one of the most effective emulsifiers in the preparation of NPs. TPGS is a water-soluble derivative of natural vitamin E with a high hydrophile–lipophile balance (HLB) of 13. Its bulky structure and large surface area make it an excellent emulsifier. High encapsulation efficiency suggests that less concentration of NPs will be needed to achieve a high concentration of the contrast agents for imaging.

4.1.5 XPS

X-ray photoelectron spectroscopy (XPS) can be applied to determine the elements or components present on the surface of a compound within a depth range of 1 to 10 nm. XPS can be used to test the types of elements present on the surface of the synthesized particles. QDs contain elements such as cadmium, selenium and zinc. XPS testing on the particle surfaces for these elements can indicate whether the QDs are actually encapsulated within the particles and not merely coated on the surfaces. The particles are also grinded to expose the contents within and sent for XPS testing again as a control to ascertain that QDs is present within the particles. Similarly, the

tests are repeated to test for iron to ascertain if IO (made up of iron) is present on the surface or inside the particles.

Figure 4.2 shows XPS result indicating no cadmium (no peaks) on particle surfaces. When the particles are grinded (exposing the contents) and tested again using XPS, the result (Figure 4.3) shows 2 peaks at 401 eV and 408 eV binding energies, indicating that cadmium is present. Test results for selenium and zinc show similar results.

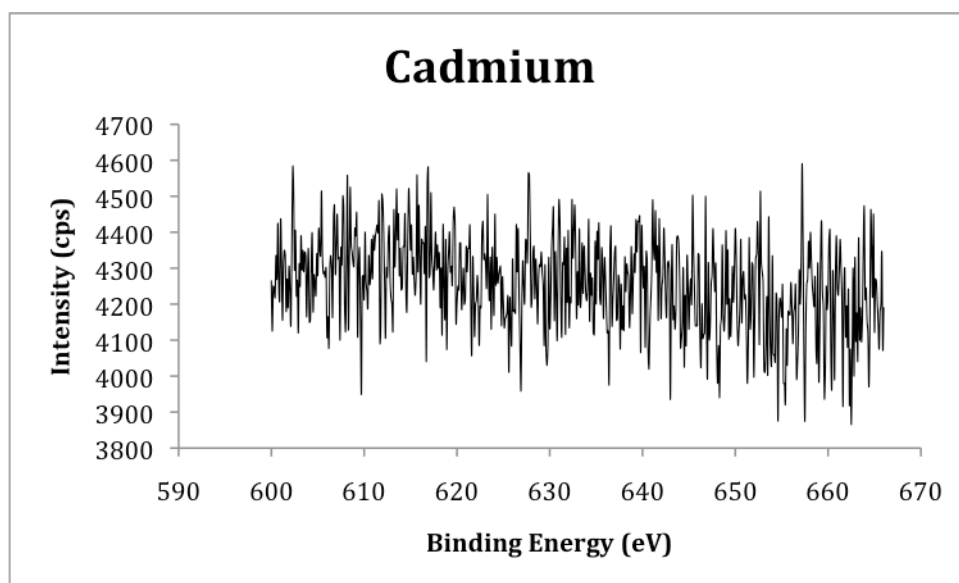


Figure 4.2: Particle XPS result for Cd showing no peaks (absence of Cd).

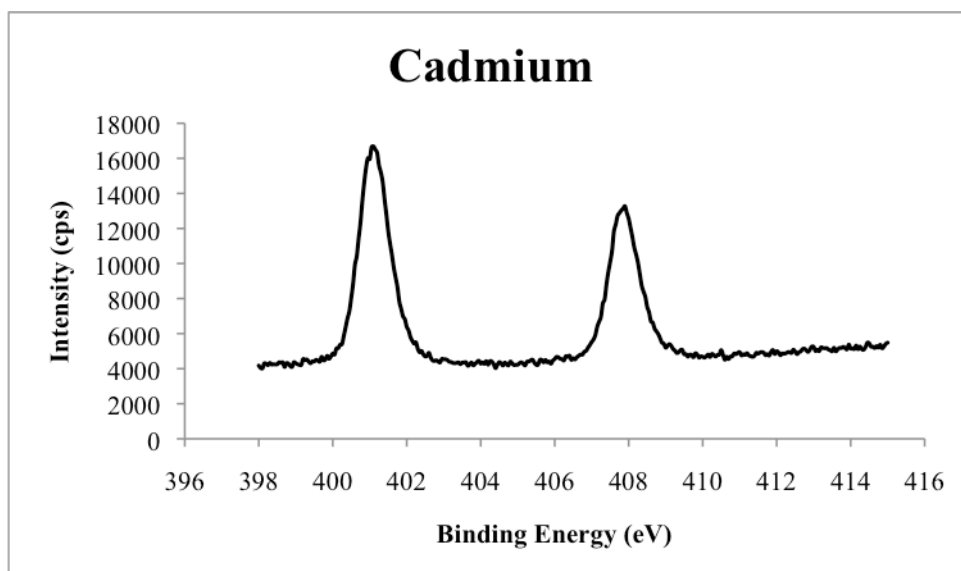


Figure 4.3: Grinded particle XPS for Cd showing 2 peaks (presence of Cd).

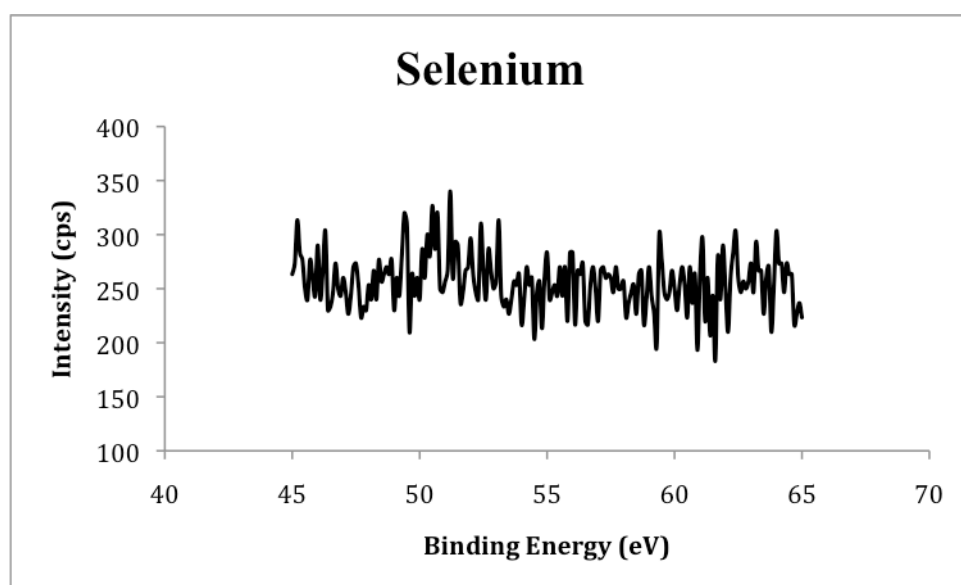


Figure 4.4: Particle XPS result for Se showing no peaks (absence of Se).

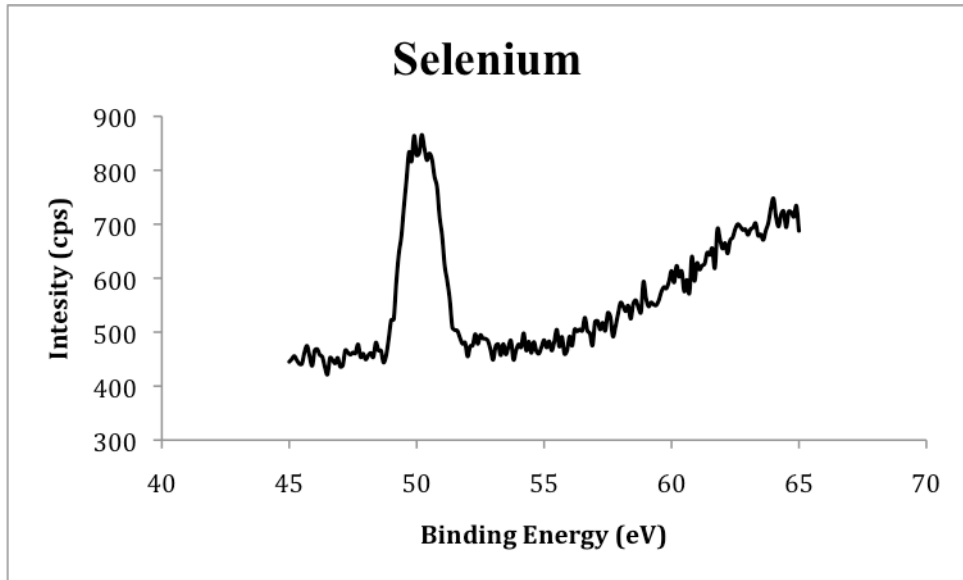


Figure 4.5: Grinded particle XPS for Se showing 1 peak (presence of Se).

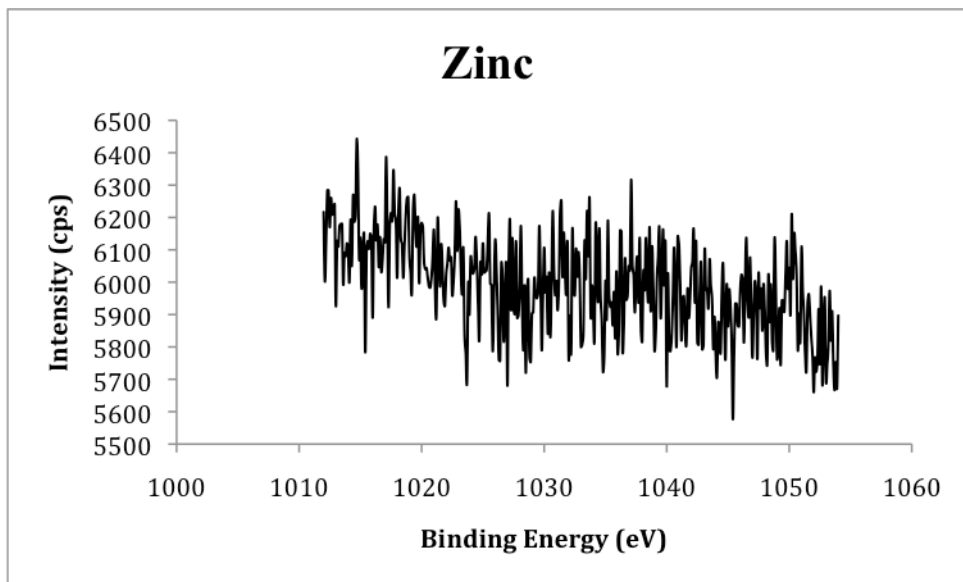


Figure 4.6: Particle XPS result for Zn showing no peaks (absence of Zn).

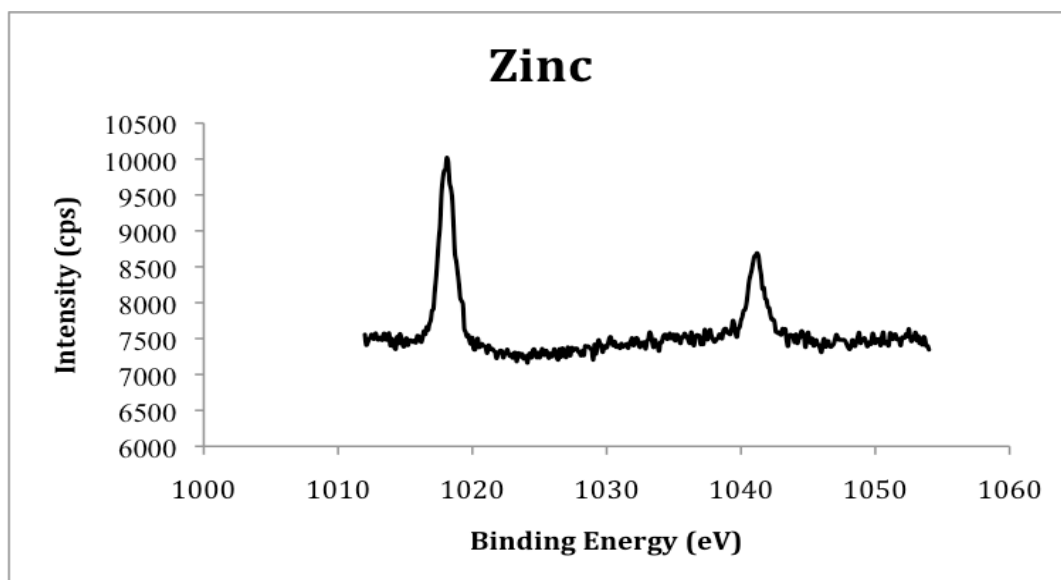


Figure 4.7: Grinded particle XPS for Zn showing 2 peaks (presence of Zn).

Figure 4.4 and 4.6 show XPS results also indicate no selenium and zinc on particle surfaces respectively. Thus, it can be concluded that there are no QDs found on the surface of the nanoparticles. Figure 4.5 shows a peak at 50 eV binding energy level indicating the presence of selenium within the particle. Figure 4.7 shows peaks at 1019 eV and 1041 eV indicating the presence of zinc within the particle. This shows that the QDs detected using ICP-MS previously were indeed all from within the particles and not merely on the surfaces.

Figure 4.8 shows XPS result indicating no iron present on the particle surfaces. Figure 4.9 shows XPS result with 2 peaks at 709 eV and 723 eV binding energy levels indicating the presence of iron. This indicates that IO present in the nanoparticles is all encapsulated within the particles and not on the particle surfaces. Thus, it can be concluded that both QDs and IO are successfully encapsulated within the nanoparticles and not merely coated on the surfaces.

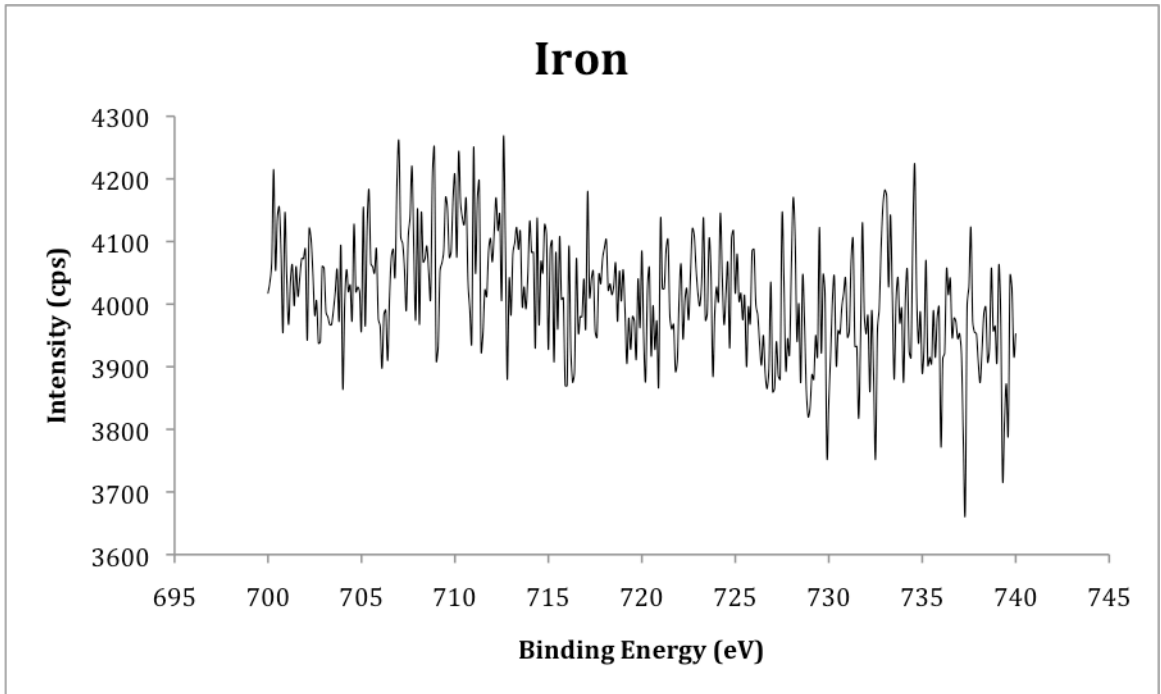


Figure 4.8: Particle XPS result for Fe showing no peaks (absence of Fe).

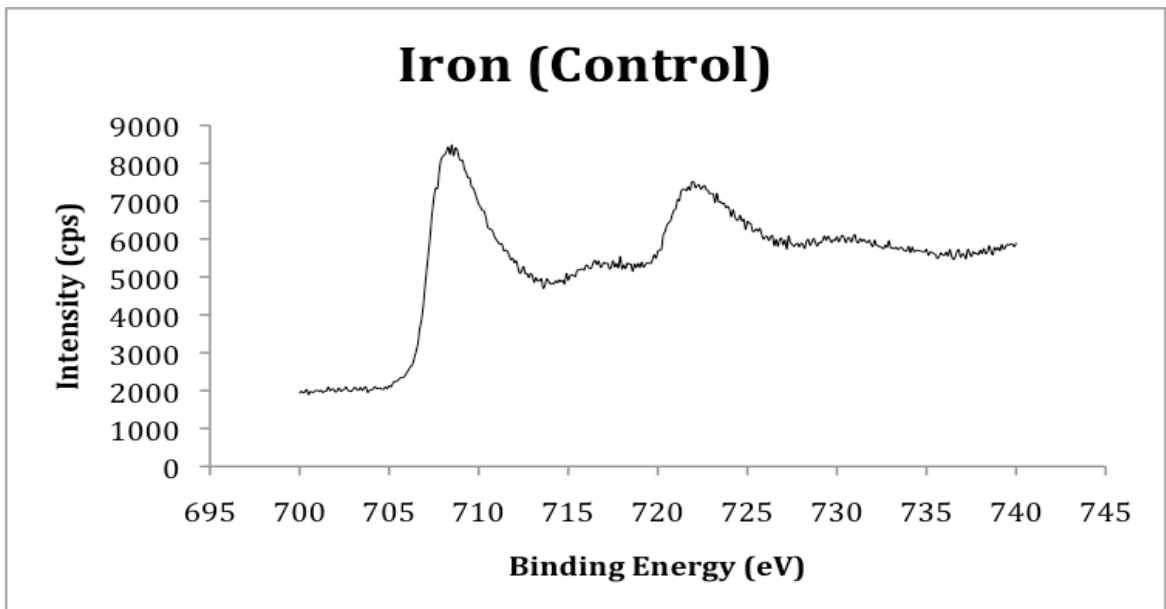


Figure 4.9: Grinded particle XPS for Fe showing 2 peaks (presence of Fe).

4.2 Cell Line Experiment

4.2.1 *In vitro* cellular uptake of NPs

4.2.1.1 Qualitative study

Figure 4.10 shows confocal laser scanning microscopy (CLSM) of MCF-7 cells after 4 h treatment with the QDs and IO-loaded PLA-TPGS NPs at 37 °C, which were diluted to the NPs concentration with QDs equivalent to 1 µg Cd in 1 mL of media. The intensity coded (red for QDs and blue for DAPI) channels show the fluorescence. Figure 4.10B shows that the nuclei of the cells were effectively stained blue by DAPI. Figure 4.10C shows the cytoplasm of the cells emitting red coded fluorescence distinctive of QDs in the NPs, proving that the NPs have been successfully taken up into the cells.

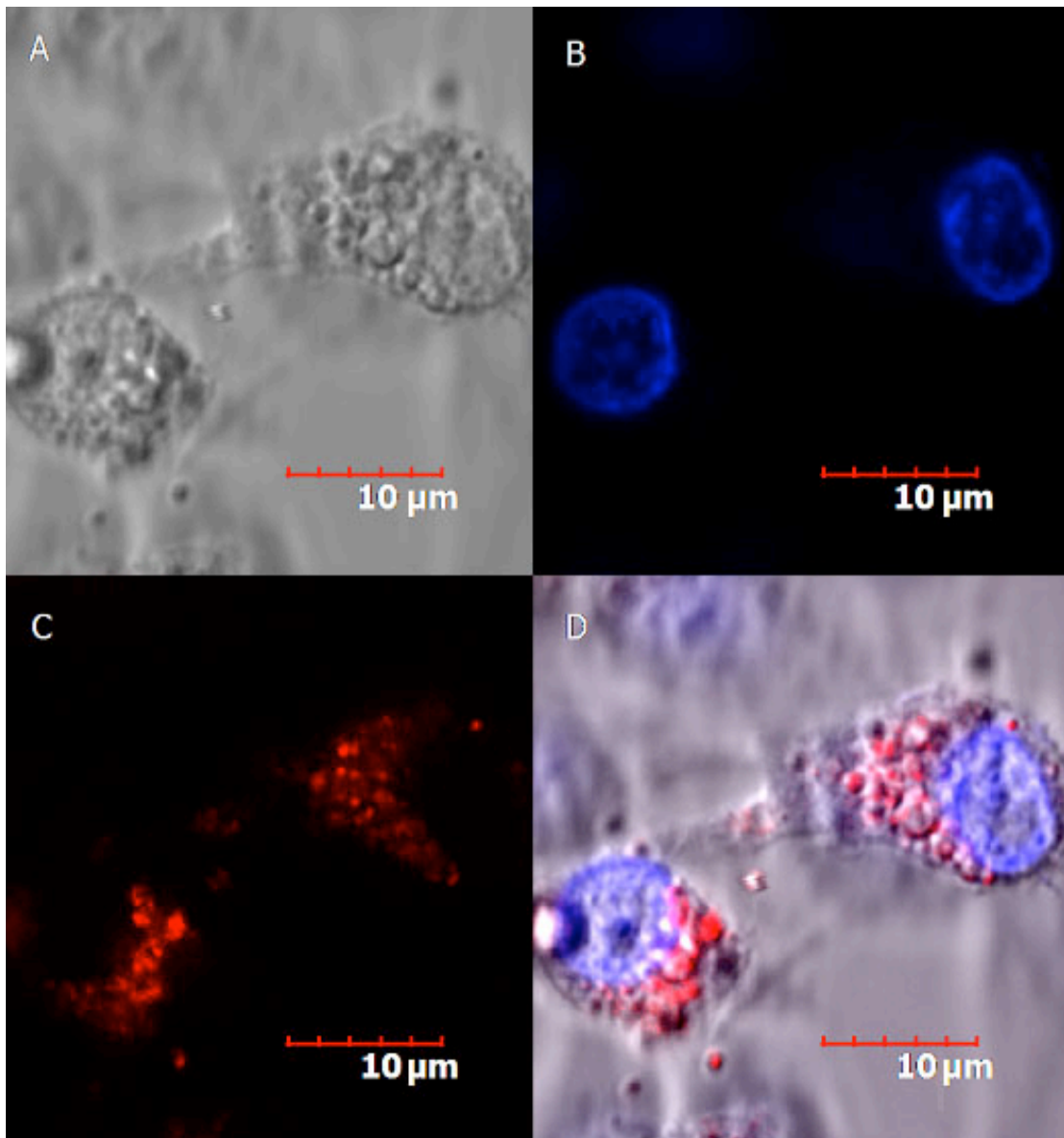


Figure 4.10: CLSM images of MCF-7 cells treated with the QDs and IOs-loaded PLA-TPGS NPs *in vitro* (scale bar = 10 μm). A: Bright field image of cells. B: Blue coded DAPI stained nuclei. C: Red coded QD from NPs in cytoplasm. D: Complete overlapped image.

4.2.1.2 Quantitative study

Figure 4.11 shows the respective fluorescence emission intensity of MCF-7 cells incubated for 1, 2 and 4 h in 100 μ L of the QDs and IO-loaded PLA-TPGS NPs at the nanoparticle concentrations containing 1 μ g/mL Cd, 0.5 μ g/mL Cd and 0.25 μ g/mL Cd respectively dispersed in medium. The readings were taken with a multiplate reader and the results were compared against the controls. The percentage uptake efficiency results of the cells treated with the NPs formulation at the various concentrations were calculated and displayed in Figure 4.11. From this graph, it is evident that the percentage uptake efficiency of the NPs formulation increases with increasing the nanoparticle concentrations. Furthermore, the percentage uptake efficiency was observed to be high at 40% - 50% within the first 4 h even at very low concentration. This shows that the PLA-TPGS NPs formulation of IOs and QDs indeed falls within suitable dimensions for cellular uptake. This also suggests that such a NPs formulation has great potential to passively deliver the contrast agents effectively into the tumor cells for better imaging.

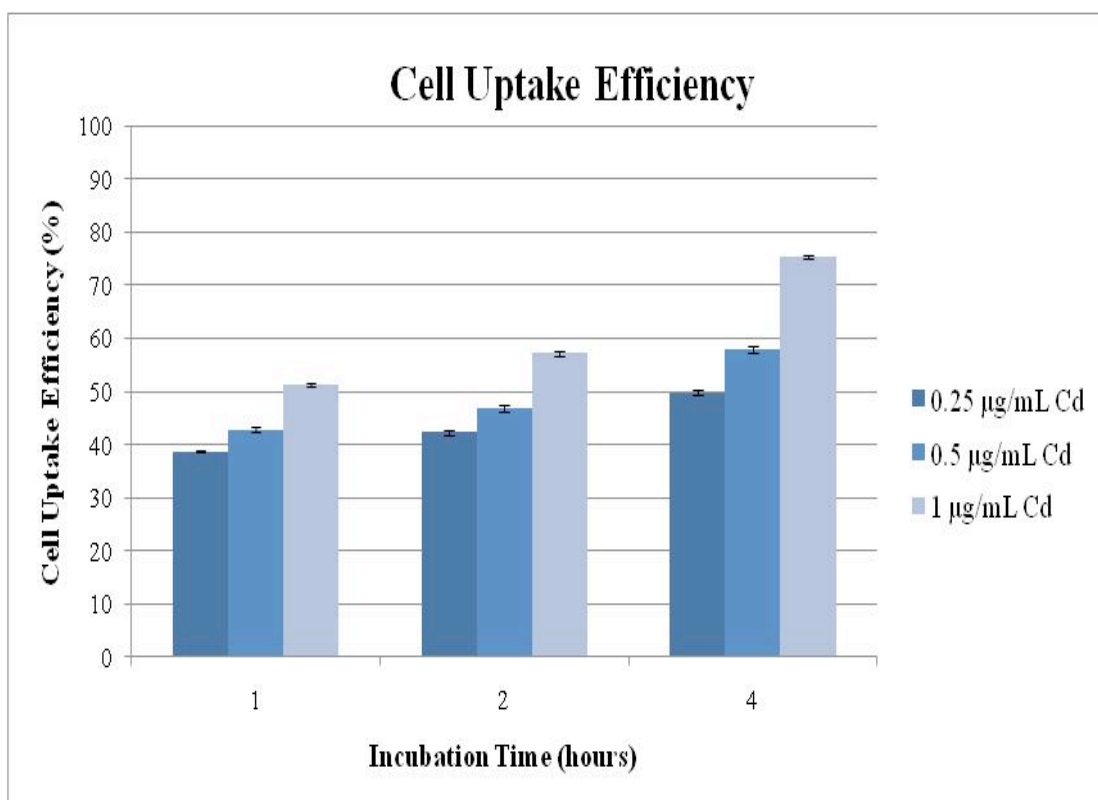


Figure 4.11: Cellular uptake efficiency of the MCF-7 cancer cells after 1, 2 and 4 h treatment with 100 µL of the QDs and IO-loaded PLA-TPGS NPs of concentrations containing 1 µg/mL Cd, 0.5 µg/mL Cd and 0.25 µg/mL Cd respectively dispersed in medium.

4.2.2 *In vitro* Cytotoxicity

QDs' toxicity has posed to be a problem for their usage. Our results further confirm that IOs may also cause substantial toxicity, which was found in our earlier research (Wang Y et al., 2008). In fact, the cadmium present in the QDs, if released, could become seriously toxic to biological cells (Celik A et al., 2005). One practical solution for such toxicity problem of QDs and IOs used as probes for imaging is to apply nanoparticles of biodegradable polymers to encapsulate them as a shield from the cellular environment. The polymer chosen as the encapsulating medium in this research is PLA-TPGS, which may have better effects than any other biodegradable polymer or co-polymer. PLA is FDA approved for clinical applications while TPGS is derived from naturally occurring vitamin E, *i.e.* a PEGylated Vitamin E. Thus, encapsulation of QDs and IOs in polymer matrix of PLA-TPGS reduces toxicity, enabling their usage for *in vivo* studies. In the *in vitro* cytotoxicity study, MCF-7 cells were treated with the synthesized QDs and IOs-loaded PLA-TPGS NPs, the free QDs and the free IOs (Resovist®) for a period of 24 h and 48 h respectively to make comparison of their cytotoxicity. The result of the cell viability expressed in percentage cell viability is shown in Fig 4.12. It can be seen from this graph that after 24 h treatment, the viability of the cells treated with the QDs and IOs-loaded PLA-TPGS nanoparticles at the designated nanoparticle concentrations was 95.4% in comparison with 81.3% for the same amount of QDs alone and 80.5% for the same amount of the IOs. Alternatively, the mortality of the cells treated with the QDs and IOs-loaded PLA-TPGS nanoparticles at the designated nanoparticle concentrations was 4.6% in comparison with 18.7% for the same amount of QDs alone and 19.5% for the same amount of the IOs. This shows that the free QDs and IO together may have about 8.3 times the cytotoxicity of the PLA-TPGS nanoparticles formulation

after 24-hour treatment. After 48 h treatment, the viability of the cells treated with the free QDs and IO were 78.1% and 78.5% (thus 21.9% and 21.5% mortality) respectively while that of the cells treated with the PLA-TPGS nanoparticle formulation of the same amount of QDs and IO was 92.0% (thus 8.0% mortality). This shows that the free QDs and IO together may have about 5.43 times the cytotoxicity of the PLA-TPGS nanoparticles formulation after 48-hour treatment.

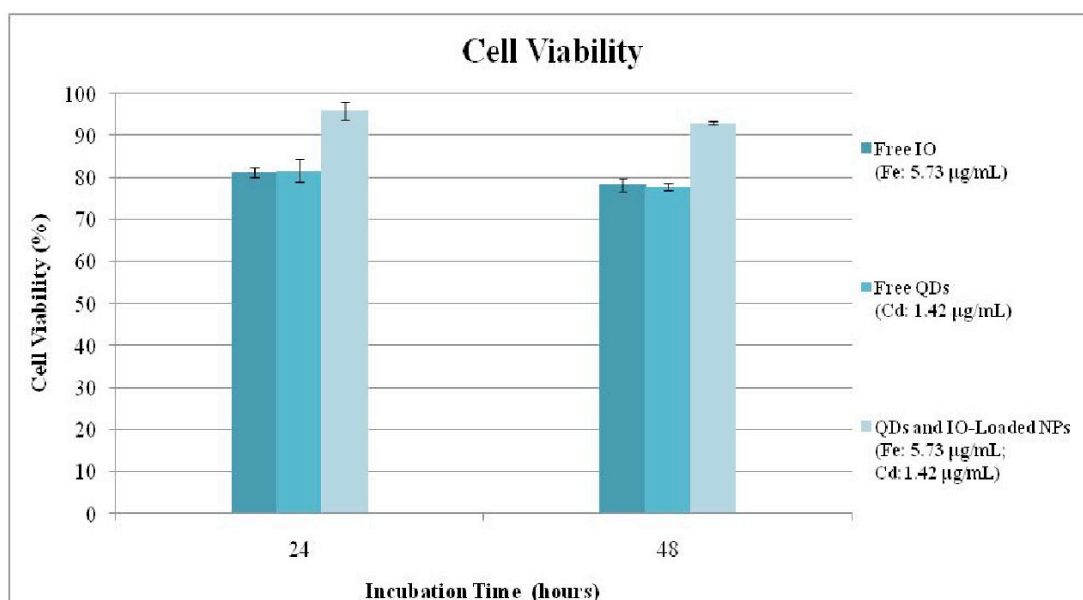


Figure 4.12: *In vitro* viability of MCF-7 cells after 24 and 48-hour treatment with the free IO, the free QDs (containing 1.42 µg/mL Cd), the free IO (containing 5.73 µg/mL Fe), and the QDs and IOs-loaded PLA-TPGS NPs (containing 1.42 µg/mL Cd and 5.73 µg/mL Fe) respectively dispersed in the medium.

4.3 Animal Study

Multimodal probes formulated in biodegradable polymers provide excellent biocompatibility and stealth from the RES system. We show in this work a series of proof-of-concept experimental results for the PLA-TPGS nanoparticles formulation of QDs and IOs to realize a practical and effective way for multimodal imaging of cancer cells *in vitro* and tumor *in vivo*. Figure 4.13 shows MRI images obtained under T2 sequence of Xenograft model mice (20 g) injected with dual modal probe (6.0 mg Fe/kg and 1.5 mg Cd/kg).

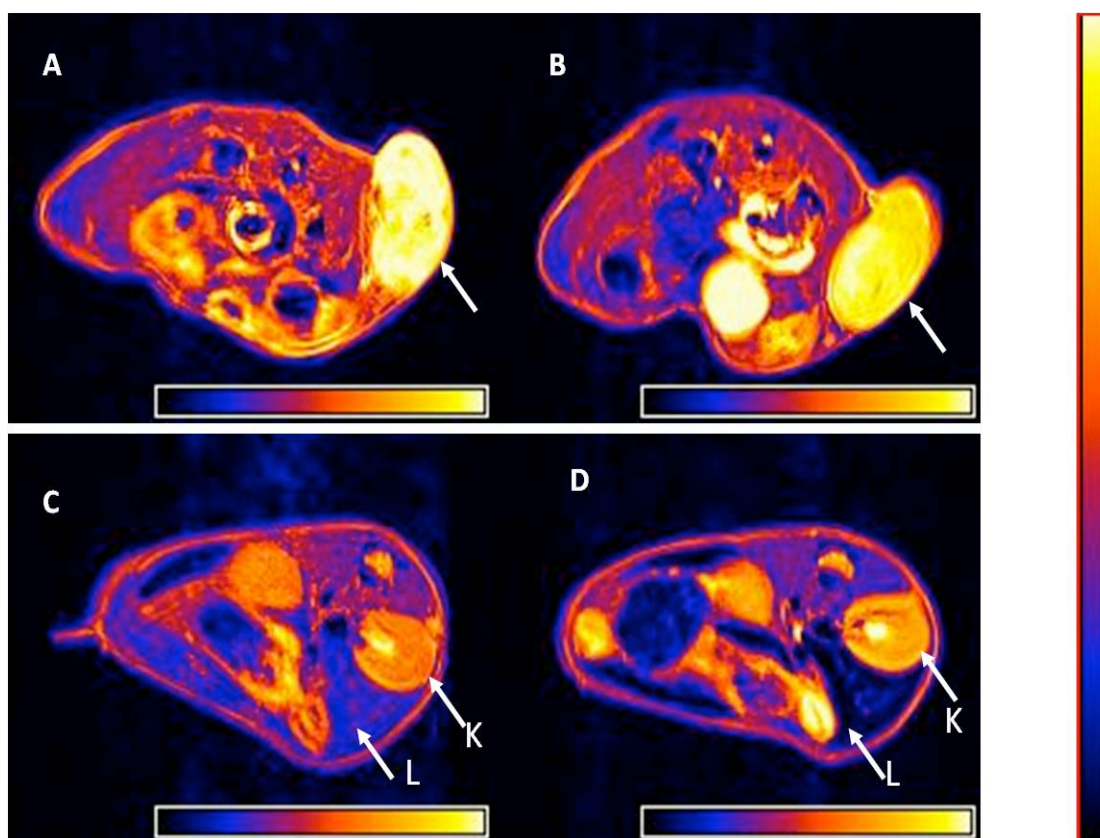


Figure 4.13: Axial MRI image sections of the MCF-7 grafted tumor bearing mice. Images A and B show the part of the tumor (shown by the arrow) before and after 6 hours of administration of the QDs and IOs-loaded PLA-TPGS NPs into the mice.

Images C and D show the kidney (K) and liver (L) part of the mice before and 6 hours after the administration of the PLA-TPGS NPs formulation of QDS and IOs (dosage: 1.5 mg of Cd/kg of body weight or equivalent of 6.0 mg of Fe/kg body weight). The decrease in intensity in the regions of the tumor and liver can be noticed in comparison with the color scale shown aside.

The images were colour mapped using MRIcro (Chris Rorden © 1999-2005). IOs injected influence T2 and thus reduced the signal intensity at the site of accumulation. This can be seen in the MRI images in Figure 4.13, displaying a signal reduction in the regions of tumor, liver and kidney after 6 h. A signal reduction of 10% was observed in the tumor. In comparison, a greater percent of signal reduction of about 50% was observed in the liver. In addition, signal reduction in the kidney was observed more at the medullar region of the kidney than at the cortical region. The results were similar to those reported by Prashant et al. ([Prashant C et al., 2010](#)).

The uptake of the nanoparticles can be a result of passive targeting of the nanoparticles in the tumor due to its enhanced permeation and retention properties. However, there were not considerable differences in other parts of the viscera according to the MRI images. Though the images were acquired non-invasively with great anatomical resolution providing the possibility to view the animal body at great depths, these findings were actually restricted to a resolution of 1 μm (maximum that can be achieved by MRI).

Figure 4.14 shows the fluorescent intensity *ex vivo* images of the various organs of the mice injected with the dual modal probes. *Ex vivo* images were acquired because the fluorescence of the respective organs obtained could be hindered due to the presence of skin, misrepresenting the actual intensities given out by the organs. The percentage

fluorescent intensity increase in the organs is directly proportional to the amount of the nanoparticle accumulations. The PLA-TPGS NPs formulation was injected into mice at a dosage of 6.0 mg Fe/kg (equivalent of 1.5 mg Cd/kg). After 6 h, the mice were sacrificed; their organs were harvested for fluorescent imaging. Figure 4.14 shows the result of the fluorescent imaging of the organs. The percentage increase in fluorescent intensities of the various organs were then calculated and plotted in Figure 4.15 to investigate the biodistribution of the NPs after being injected into the mice.

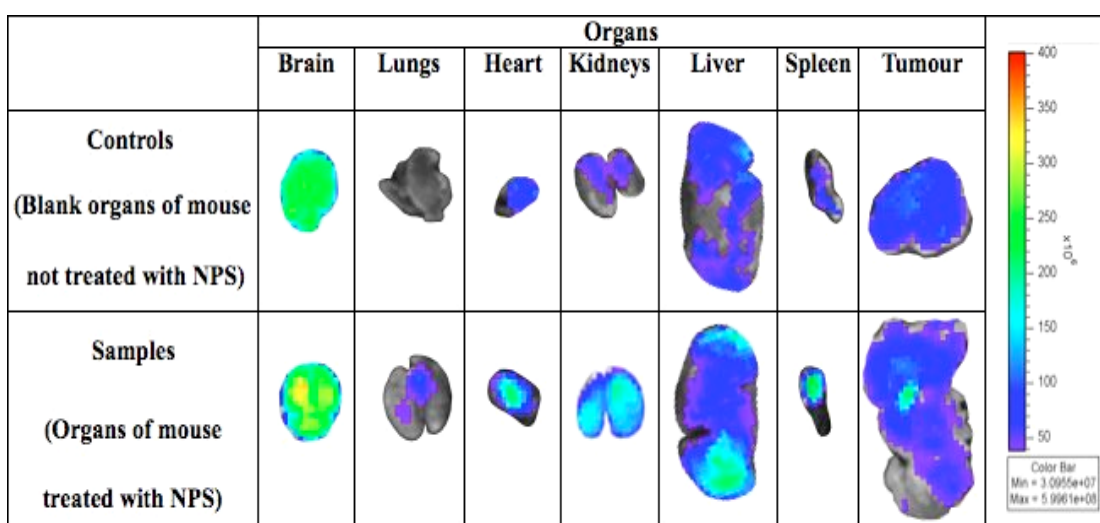


Figure 4.14: Fluorescent Images of the various organs. Upper row: control. Lower row: Organs of the mouse treated with the QDs and IOs-loaded PLA-TPGS NPs (dosage: 1.5 mg of Cd/kg of body weight or equivalent of 6.0 mg of Fe/kg body weight).

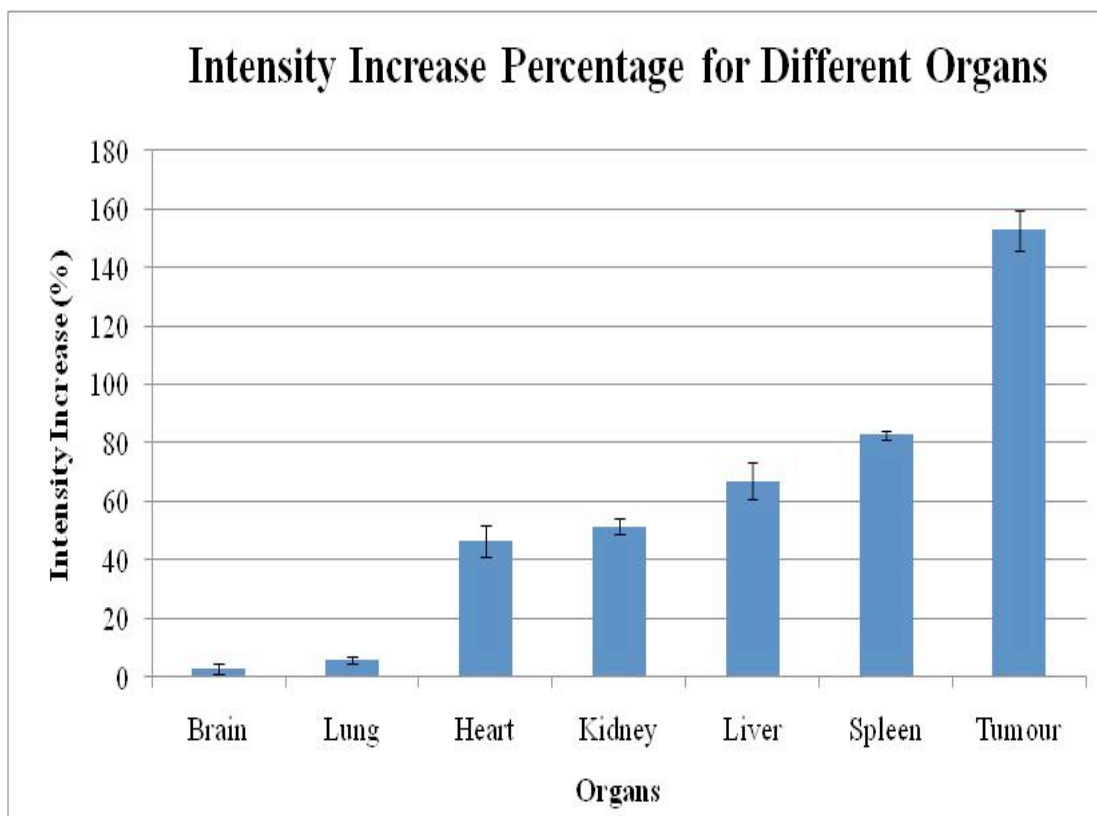


Figure 4.15: Fluorescence intensity increase percentage for the various organs of the mice treated with the QDs and IOs-loaded PLA-TPGS NPs (dosage: 1.5 mg of Cd/kg of body weight or equivalent of 6.0 mg of Fe/kg body weight).

As the liver, kidneys and spleen act as major detoxifying organs, they are expected to contain high concentrations of NPs. However, it is important to observe that there is about 153% increase in fluorescent intensity in the tumor. This shows that the tumor has passively uptaken a large amount of the NPs due to its poor drainage system. Hence, this exhibits how the PLA-TPGS NPs formulation could be used to detect and image tumors *in vitro* and *in vivo*. From Figure 4.15, it can be seen that fluorescent intensity percentage increase is 67% in the liver, 52% in the kidney and 153% in the tumor, which complements the finding from the MRI. The resolution of the fluorescence is greatly improved as shown in Figure 4.16, 4.17 and 4.18 (confocal).

Figure 4.16D, 4.16E and 4.16F show the images of the liver section of a mouse

treated with the QDs and IOs-loaded PLA-TPGS NPs compared with a set of blank images (Figure 4.16A, 4.16B and 4.16C).

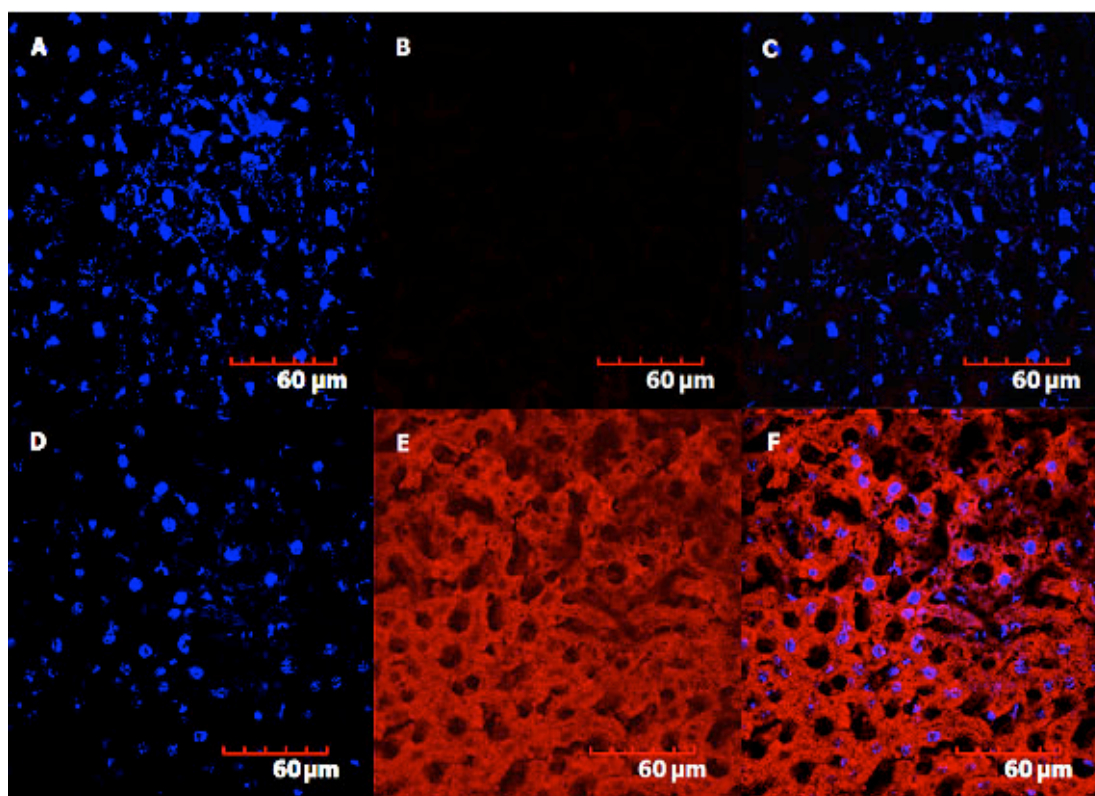


Figure 4.16: Confocal laser scanning microscopy sections of the mouse liver (scale bar = 60 μm). Images A, B and C show the liver sections of the control with no treatment. A: Blue coded DAPI stained nuclei. B: Red channel detection showing no signal due to absence of QDs. C: Complete overlapped image of A and B. Images D, E and F show the liver sections of the mouse treated with the QDs and IOs loaded PLA-TPGS NPs. D: Blue coded DAPI stained nuclei. E: Red coded QD from NPs in cytoplasm. F: Complete overlapped image.

Images 4.16A and 4.16D show the blue coded channels. Images 4.16B and 4.16E show the red coded channels. Images 4.16C and 4.16F had the red and blue coded channels overlapped. Both images of 4.16A and 4.16D registered blue signals,

representing the nuclei of the liver cells stained blue by DAPI. Image 4.16B registered no red fluorescence indicating that QDs were absent. Image 4.16E however registered red fluorescence in the cytoplasm of the liver cells, indicating that QDs were present and suggesting that the NPs have been uptaken in the liver cells of the mouse. Similar findings were arrived at in the kidney sections (Figure 4.17) and the tumor sections (Figure 4.18). Therefore, in summary, the QDs and IOs-loaded PLA-TPGS NPs, when injected into the mice, were able to travel to and get internalized by the various organ cells as well as by the tumor cells.

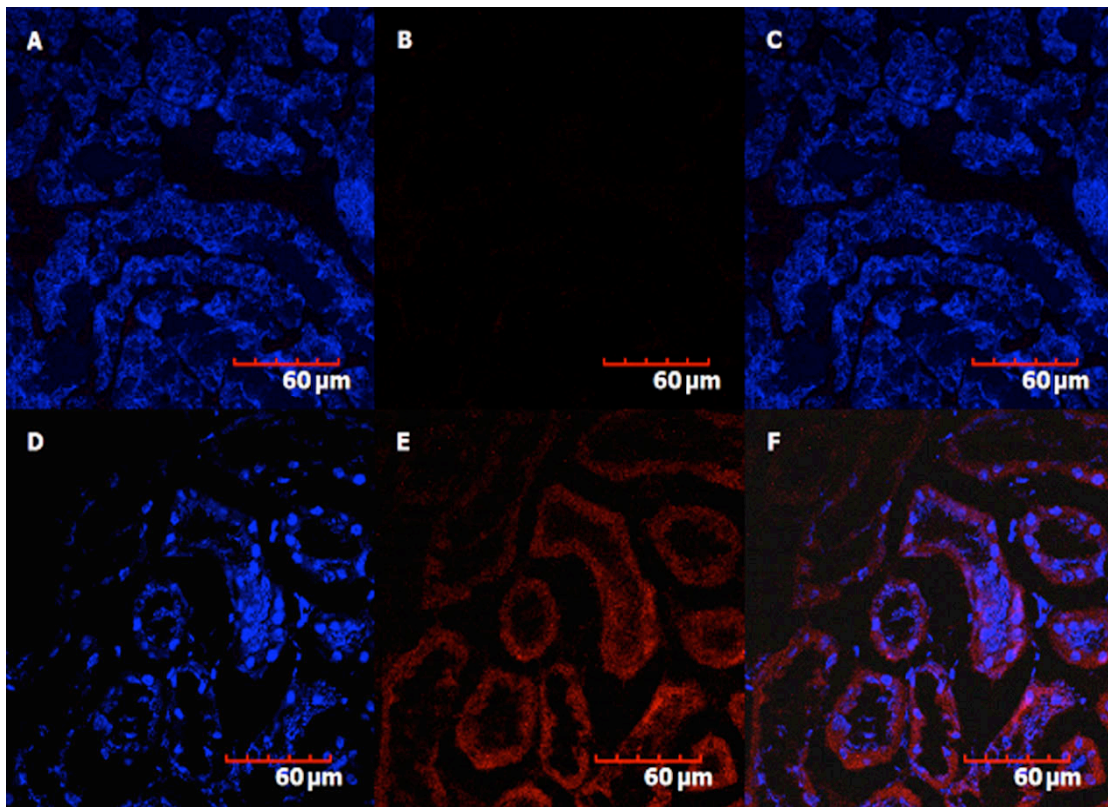


Figure 4.17: Confocal laser scanning microscopy sections of the mouse kidney sections (scale bar = 60 μm). Images A, B and C show the kidney sections of the control with no treatment. A: Blue coded DAPI stained nuclei. B: Red channel detection showing no signal due to absence of QDs. C: Complete overlapped image of A and B. Images D, E and F show the kidney sections of the mouse treated with the

QDs and IOs loaded PLA-TPGS NPs. D: Blue coded DAPI stained nuclei. E: Red coded QD from NPs in cytoplasm. F: Complete overlapped image.

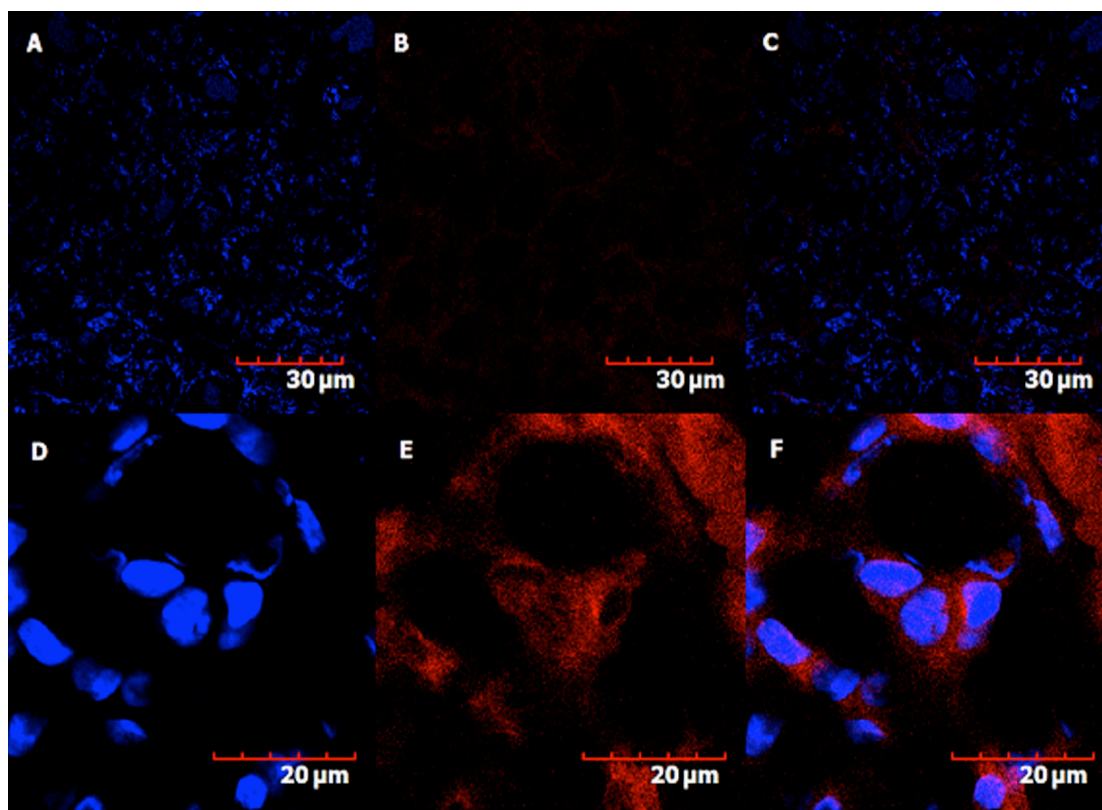


Figure 4.18: Confocal laser scanning microscopy sections of the mouse tumor sections. Images A, B and C (scale bar = 30 μm) show the tumor sections of the control with no treatment. A: Blue coded DAPI stained nuclei. B: Red channel detection showing no signal due to absence of QDs. C: Complete overlapped image of A and B. Images D, E and F (scale bar = 20 μm) show the tumor sections of the mouse treated with the QDs and IOs loaded PLA-TPGS NPs. D: Blue coded DAPI stained nuclei. E: Red coded QD from NPs in cytoplasm. F: Complete overlapped image.

From these confocal images, it was clearly observed that the QDs and IOs-loaded PLA-TPGS NPs were internalized into the cytoplasmic regions of the various organ

cells. The findings of the MRI were thus confirmed by the confocal microscopy, wherein the medullar region of the kidney showed fluorescence and not the cortical region. Thus it shows that the developed dual modal probe works. It has been exhibited that co-encapsulating both the QDs and IO contrast agents into a single polymeric nanoparticle probe has resulted in a probe that exhibits the advantages of both the individual contrast agents. This poses to be the key to limitless possibilities in terms of applications for human imagery. Such a system of dual modality can be useful for pre- and during surgical treatment of cancer (Kircher MF et al., 2003; Mulder WJM et al., 2007). The non-invasive MRI imaging can ensure pre-operative identification of cancer while the less complicated fluorescent imaging techniques on operative procedure can ensure demarcation of tumor sites and delineation of healthy and normal cells. Moreover a method of molecular tracking can also be performed (Tada H, et al., 2007). MRI and fluorescence imaging on white mice induced with MCF-7 tumors injected with the nanoparticles were able to detect the locations of the tumors easily due to the passive targeting effect of the particles at the tumor sites, enhancing the contrast effect at the tumor locations. That suggested the possibility of using merely a single injection of the nanoparticles to utilize both MRI and fluorescence imaging for a patient to effectively detect any tumors within him. The results of both imaging modes can be cross-referenced to confirm the presence of a tumor at the same particular site imaged using both systems. In that way, early staged cancer not only would not be overlooked, but also could be more effectively detected and hence easily treated. Therefore, our results show the effectiveness of the designed dual modal probe in imaging tumors in the animal. Further refinements to this multimodal probe will realize its full potential in the imaging of the human body through various application possibilities.

CHAPTER 5: OUTLOOK

The work presented in this thesis describes a multimodal imaging approach by co-encapsulating both IO and QDs to make use of both MRI and fluorescence imaging. This imaging system strikes at detecting cancer at its earliest stage where detection may be overlooked easily due to limitations with the use of only one imaging mode. This work can potentially be very useful for cancer imaging. However, it is still in its preliminary stage where some issues must first be addressed.

The first and most crucial issue is the stability of the nanoparticles in the human body and their behavior within the human body until they are expelled from the body. The ideal scenario will definitely be that the particles do not break down to release the IO and QDs contained within. However, if the particles do break down to release the contrast agents before being expelled out of the body, the behaviors of the QDs should be investigated on until they were removed from the body. This is due to the toxicity of the QDs used. QDs commonly consist of cadmium and selenium in their core metalloid complexes. They will exhibit some toxic effects when they are broken down to their ionic forms. In general, the tricky situation is that not all QDs are alike. Therefore, it is impossible to categorize all engineered QDs into the same group of nanomaterials. QDs ADME and toxicity is based on various different factors derived from both inherent physicochemical properties and environmental conditions. These factors include QDs size, charge, concentration, outer coating bioactivity (capping material and functional groups), and oxidative, photolytic, and mechanical stability ([Ron Hardman, 2006](#)).

Physicochemical property of a type of QDs affects its toxicity and each individual type of QDs possesses its own unique physicochemical properties. In general, there are discrepancies in the current available literatures regarding the toxicity of QDs.

This can be due to the lack of toxicology-based studies, the variety of QD dosage/exposure concentrations reported in the various available literatures, and the widely varying physicochemical properties of individual QDs. There are limited studies specifically designed for toxicological assessment of QDs. Hence, it is important to conduct a thorough toxicity assessment on the particular QDs used in this work to verify if it is suitable to be used as described in this thesis for human application. In the event, after toxicity assessment, that the particular QDs used in this work is not suitable, alternative types of QDs can be tested to find the most suitable QDs for the application described in this work. Furthermore, future optimization work can be done on parameters such as the concentrations and dosages of QDs to refine the imaging system.

The second issue of this developed system is that it only has passive targeting effect in tumors. To enable even more enhanced detection of tumors, the surfaces of the synthesized IO and QDs encapsulated PLA-TPGS nanoparticles can be decorated with ligands that are specific to receptors found in abundance on the cancer tumors to be targeted. In this way, even very small tumors can be detected effectively and efficiently.

CHAPTER 6: CONCLUSION

I have developed an imaging system by co-encapsulation QDs and IOs in nanoparticles of PLA-TPGS copolymers for both MRI and fluorescent imaging.

LLS, TEM, ICP-MS and XPS were used to characterize the developed particles. The size and size distribution of the nanoparticles (measured by laser light scattering) were around 325.8 nm in diameter with a PDI of 0.204. This shows that the particles were quite uniform in size and within the optimum cellular uptake range. They were negatively charged at about -37.3 mV suggesting that they were stable in solution.

TEM images of QDs and IOs-loaded PLA-TPGS nanoparticles showed spherical well-formed nanoparticle with dark spots (QDs and IOs) encapsulated uniformly in the polymeric nanoparticle. QDs were elliptically shaped while the IOs were spherically shaped.

ICP-MS was used to measure the amount of Cd and Fe contents present in the nanoparticles to quantify the amount of the QDs and IO inside. The encapsulation efficiency of QDs was found to be about 45% while that of IOs was about 60%. The encapsulation efficiencies of QDs and IOs were relatively high. High encapsulation efficiency suggests that less concentration of NPs will be needed to achieve a high concentration of the contrast agents for imaging.

XPS was used to test the types of elements present on the surface of the synthesized particles. QDs contain elements such as cadmium, selenium and zinc while IO contains iron. XPS testing on the particle surfaces for these elements can indicate whether the QDs and IO were actually encapsulated within the particles and not merely coated on the surfaces. The particles were also grinded to expose the contents within and sent for XPS testing again as a control. XPS results revealed that cadmium, selenium, zinc and iron were only detected within and not on the surfaces

of the particles. That concluded successful encapsulation of QDs and IO within the nanoparticles.

In Vitro tests were then conducted to find out the cellular uptake of the particles in MCF-7 breast cancer cells. Cytotoxicity tests were also conducted on the cells to find out the toxicity of the particles. For the qualitative *in vitro* cell uptake study, MCF-7 cells were treated with the QDs and IO-loaded PLA-TPGS NPs at 37 °C for 4 h. The NPs concentration used was the QDs equivalent to 1 µg Cd in 1 mL of media. Confocal laser scanning microscopy on the treated cells showed red coded fluorescence distinctive of QDs in the NPs in the cytoplasm of the cells, proving that the NPs have been successfully taken up into the cells. For the quantitative cell uptake study, MCF-7 cells were incubated for 1, 2 and 4 h in 100 µL of the QDs and IO-loaded PLA-TPGS NPs at the nanoparticle concentrations containing 1 µg/mL Cd, 0.5 µg/mL Cd and 0.25 µg/mL Cd respectively dispersed in medium. The readings were taken with a multiplate reader and the results were compared against the controls. The percentage uptake efficiency results of the cells treated with the NPs formulation at the various concentrations were calculated and charted in a graph. The results showed that the percentage uptake efficiency of the NPs formulation increases with increasing nanoparticle concentrations. The percentage uptake efficiency was observed to be high at 40 - 50% within the first 4 h even at very low concentration showing that the formulated NPs indeed falls within suitable dimensions for cellular uptake.

In the *in vitro* cytotoxicity study, MCF-7 cells were treated with the synthesized QDs and IOs-loaded PLA-TPGS NPs, the free QDs and the free IOs (Resovist®) for a period of 24 and 48 h respectively to make comparison of their cytotoxicity. The results showed that after 24 h treatment, the viability of the cells treated with the QDs

and IOs-loaded PLA-TPGS nanoparticles at the designated nanoparticle concentrations was 95.4% in comparison with 81.3% for the same amount of QDs alone and 80.5% for the same amount of the IOs. Alternatively, the mortality of the cells treated with the QDs and IOs-loaded PLA-TPGS nanoparticles at the designated nanoparticle concentrations was 4.6% in comparison with 18.7% for the same amount of QDs alone and 19.5% for the same amount of the IOs. This shows that the free QDs and IO together may have about 8.3 times the cytotoxicity of the PLA-TPGS nanoparticles formulation after 24-hour treatment. After 48 h treatment, the viability of the cells treated with the free QDs and IO were 78.1% and 78.5% (thus 21.9% and 21.5% mortality) respectively while that of the cells treated with the PLA-TPGS nanoparticle formulation of the same amount of QDs and IO was 92.0% (thus 8.0% mortality). This shows that the free QDs and IO together may have about 5.43 times the cytotoxicity of the PLA-TPGS nanoparticles formulation after 48-hour treatment.

Multimodal probes formulated in biodegradable polymers provide excellent biocompatibility and stealth from the RES system. A series of proof-of-concept experiments was conducted on white mice with the formulated particles to show that multimodal imaging of cancer cells *in vitro* and tumor *in vivo* is practical and effective. MRI images were taken under T2 sequence of Xenograft model mice (20 g mice with induced MCF-7 cancer tumor) injected with dual modal probe (6.0 mg Fe/kg and 1.5 mg Cd/kg). IOs injected influence T2 and thus reduced the signal intensity at the site of accumulation. That can be seen in the MRI images displaying a signal reduction in the regions of tumor, liver and kidney after 6 h. A signal reduction of 10% was observed in the tumor. In comparison, a greater percent of signal reduction of about 50% was observed in the liver. In addition, signal reduction in the kidney was observed more at the medullar region of the kidney than at the cortical

region. The uptake of the nanoparticles can be a result of passive targeting of the nanoparticles in the tumor due to its enhanced permeation and retention properties.

The mice used were then harvested of their organs, which were then sent for fluorescence imaging. *Ex vivo* images were acquired because the fluorescence of the respective organs obtained could be hindered due to the presence of skin, misrepresenting the actual intensities given out by the organs. The percentage fluorescent intensity increase in the organs is directly proportional to the amount of the nanoparticle accumulations. The percentage increase in fluorescent intensities of the various organs were then calculated and plotted in a graph to investigate the biodistribution of the NPs after being injected into the mice.

As the liver, kidneys and spleen act as major detoxifying organs, they were expected to contain high concentrations of NPs. There was about 153% increase in fluorescent intensity in the tumor. That suggested that the tumor has passively uptaken a large amount of the NPs due to its poor drainage system. That exhibited how the PLA-TPGS NPs formulation could be used to detect and image tumors *in vitro* and the tumor itself *in vivo*. It was observed that fluorescent intensity percentage increase is 67% in the liver, 52% in the kidney and 153% in the tumor, which complements the finding from the MRI. Confocal imaging of the tumor, liver and kidney sections showed QDs fluorescence from the sections, further confirming that the QDs and IOs-loaded PLA-TPGS NPs, when injected into the mice, were able to travel to and get internalized by the various organ cells as well as by the tumor cells.

The experimental results showed that the developed IO and QDs loaded PLA-TPGS nanoparticles can be effectively uptaken into cancer cells *in vitro*. *In vivo* studies on white mice also revealed that the particles could be uptaken passively into the tumor. The PLA-TPGS coating has shielded the contrast agents (IO and QDs), which were

encapsulated within from detection by the human immune system. Thus, increasing their half-life in circulation and realizing sustained and controlled delivery of imaging agents with passive targeting effects for the tumors. Such a multimodal imaging system marries the advantages of both contrast agents making the resultant probe highly sensitive with good depth penetration. This union of QDs and IO as a single probe strives to improve imaging with practical clinical feasibility.

MRI and fluorescence imaging on white mice induced with MCF-7 tumors injected with the nanoparticles were able to detect the locations of the tumors easily due to the passive targeting effect of the particles at the tumor sites, enhancing the contrast effect at the tumor locations. That suggested the possibility of merely a single injection of the nanoparticles to utilize both MRI and fluorescence imaging for a patient to effectively detect any tumors within him. The results of both imaging modals can be cross-referenced to confirm the presence of a tumor at the same particular site imaged using both systems. In that way, early staged cancer could be more effectively detected and easily treated.

The in vitro cell toxicity tests revealed that the formulated nanoparticles were significantly less toxic than the respective individual contrast agents. Free QDs and IO together have about 8.3 times and 5.43 times the cytotoxicity of the PLA-TPGS nanoparticles formulation after 24-hour and 48-hour treatments respectively. Furthermore, animal testing showed that the polymeric coating was able to protect the contrast agents from human immune system detection until they travel to the intended imagery sites. Hence showing that the coating was stable and could increase circulation time of the probe. However, the stability of the nanoparticles within the human body was not studied and thus further work can be done to investigate the stability of the nanoparticles under human body conditions. On the other hand, studies

should also be done on the stability of the IO and QDs encapsulated within the nanoparticles in event that the nanoparticles break down within the human body before being removed from the body. The stability of the contrast agents, especially the QDs, could determine the visibility of the system to be applied to human. If the QDs were to break down into toxic ionic forms before being expelled out of the human body, alternative QDs should be explored to find the most suitable QDs for this system.

MRI and fluorescent imaging have both confirmed the ability of such a nanoparticle formulation system to passively target tumor in mice. I envision further development of this technology, particularly by incorporating drugs into the nanoparticles and surface modifying the nanoparticle surfaces with targeting ligands to target corresponding kinds of cancers. This will open exciting opportunities in traceable delivery and also improve imaging to the extent that cancers can be accurately detected even at very early stages, enabling cancers to be cured before they develop into terminal stages.

CHAPTER 7: REFERENCES

Agarwal A, Tripathi PK, Tripathi S, Jain NK. Fluorescence Imaging: Applications in Drug Delivery Research. *Curr Drug Targets*. 2008;9:895-8.

Ballou B, Lagerholm BC, Ernst LA, Bruchez MP, Waggoner AS. Noninvasive imaging of quantum dots in mice. *Bioconjug Chem*. 2004;15:79-86.

BBC News. Cancer: The Facts. Retrieved on March 2, 2009 from the World Wide Web: <http://news.bbc.co.uk/2/hi/health/3444635.stm>.

Brown, C. The Independent. Suppressed report shows cancer link to GM potatoes. Retrieved on January 05, 2009 from the World Wide Web: <http://www.independent.co.uk/life-style/health-and-wellbeing/health-news/suppressed-report-shows-cancer-link-to-gm-potatoes-436673.html>.

Bruchez M, Moronne M, Gin P, Weiss S, Alivisatos AP. Semiconductor nanocrystals as fluorescent biological labels. *Science*. 1998;281:2013-6.

Cancer Research UK. Lung Cancer. Retrieved on Nov 1, 2010 from the World Wide Web: <http://info.cancerresearchuk.org/cancerstats/types/lung/?a=5441>.

Carstensen H, Muller RH, Muller BW. Particle-size, surface hydrophobicity and interaction with serum of parenteral fat emulsions and model-drug carriers as parameters related to res uptake. *Clin Nutr*. 1992;11:289-97.

Celik A, Comelekoglu U, Yalin S. A study on the investigation of cadmium chloride genotoxicity in rat bone marrow using micronucleus test and chromosome aberration analysis. *Toxicol Ind Health*. 2005;21:243-8.

Chilukuri N, Parikh K, Sun W, Naik R, Tipparaju P. Polyethylene glycosylation prolongs the circulatory stability of recombinant human butyrylcholinesterase. *Chemico-Biological Interactions*. 2005; 157–158: 115–121

Choi JH, Nguyen FT, Barone PW, Heller DA, Moll AE, Patel D, et al. Multimodal biomedical imaging with asymmetric single-walled carbon nanotube/iron oxide nanoparticle complexes. *Nano Lett*. 2007;7:861-7.

Cochran ST. Anaphylactoid reactions to radiocontrast media. *Medicine*. 2005;5:28-31.

Derfus AM, Chan WCW, Bhatia SN. Probing the cytotoxicity of semiconductor quantum dots. *Nano Lett*. 2004;4:11-8.

Dintaman JM, Silverman JA. Inhibition of P-glycoprotein by D-alpha-tocopheryl polyethylene glycol 1000 succinate (TPGS). *Pharm Res*. 1999;16:1550-6.

Donald E, Owens I, Nicholas A. Peppas Opsonization, biodistribution, and pharmacokinetics of polymeric nanoparticles. *International Journal of Pharmaceutics*. 2006; 307:93-102

Feng SS, Chien S. Chemotherapeutic engineering: Application and further development of chemical engineering principles for chemotherapy of cancer and other diseases. *Chem Eng Sci*. 2003;58:4087-114.

Frank M, Fries L. The role of complement in inflammation and phagocytosis. *Immunol. Today*. 1991; 12: 322–326.

Gao XH, Cui YY, Levenson RM, Chung LWK, Nie SM. *In vivo* cancer targeting and imaging with semiconductor quantum dots. *Nat Biotechnol*. 2004;22:969-76.

Gao XH, Yang LL, Petros JA, Marshal FF, Simons JW, Nie SM. *In vivo* molecular and cellular imaging with quantum dots. *Curr Opin Biotechnol*. 2005;16:63-72.

Goldman ER, Anderson GP, Tran PT, Mattoussi H, Charles PT, Mauro JM. Conjugation of luminescent quantum dots with antibodies using an engineered adaptor protein to provide new reagents for fluoroimmunoassays. *Anal Chem*. 2002;74:841-7.

Govender T, Stolnik S, Garnett MC, Illum L, Davis SS. PLGA nanoparticles prepared by nanoprecipitation: drug loading and release studies of a water soluble drug. *Journal of Controlled Release*, 1999; 57(2): 171-185.

Green M, O'Brien P. Recent advances in the preparation of semiconductors as isolated nanometric particles: new routes to quantum dots. *Chem Commun*. 1999:2235-41.

Gref R, Minamitake Y, Peracchia MT, Trubetskoy V, Torchilin V, Langer R. Biodegradable long-circulating polymeric nanospheres. *Science*. 1994;263:1600-3.

Hwang DW, Ko HY, Lee JH, Kang H, Ryu SH, Song IC, et al. A Nucleolin-Targeted Multimodal Nanoparticle Imaging Probe for Tracking Cancer Cells Using an Aptamer. *J Nucl Med*. 2010;51:98-105.

Illum L, Davis SS. The organ uptake of intravenously administered colloidal particles can be altered using a non-ionic surfactant (Ploxxamer-338). *Febs Lett*. 1984;167:79-82.

Jackson GD, Kuzniecky RI, Pell GS. Principles of magnetic resonance imaging, in magnetic resonance in epilepsy (Second Edition), M.D, et al., Editors. Burlington: Academic Press; 2005. p. 17-28.

Jain TK, Foy SP, Erokwu B, Dimitrijevic S, Flask CA, Labhasetwar V. Magnetic resonance imaging of multifunctional pluronic stabilized iron-oxide nanoparticles in tumor-bearing mice. *Biomaterials*. 2009; 30(35): 6748-6756.

- Johnson BM, Charman WN, Porter CJ. An *in vitro* examination of the impact of polyethylene glycol 400, Pluronic P85, and vitamin E d-alpha-tocopheryl polyethylene glycol 1000 succinate on P-glycoprotein efflux and enterocyte-based metabolism in excised rat intestine. *AAPS Pharmsci.* 2002;4:E40.
- Kaul G, Amiji M. Long-circulating poly(ethylene glycol)-modified gelatin nanoparticles for intracellular delivery. *Pharm Res.* 2002;19:1061-7.
- Ke JH, Lin JJ, Carey JR, Chen JS, Chen CY, Wang LF. A specific tumor-targeting magnetofluorescent nanoprobe for dual-modality molecular imaging. *Biomaterials.* 2010;31:1707-15.
- Kim S, Lim YT, Soltesz EG, De Grand AM, Lee J, Nakayama A, et al. Near-infrared fluorescent type II quantum dots for sentinel lymph node mapping. *Nat Biotechnol.* 2004;22:93-7.
- Kircher MF, Mahmood U, King RS, Weissleder R, Josephson L. A multimodal nanoparticle for preoperative magnetic resonance imaging and intraoperative optical brain tumor delineation. *Cancer Res.* 2003;63:8122-5.
- Lee SJ, Jeong JR, Shin SC, Huh YM, Song HT, Suh JS, et al. Intracellular translocation of superparamagnetic iron oxide nanoparticles encapsulated with peptide-conjugated poly(D,L lactide-co-glycolide). *J Appl Phys.* 2005;97:10Q913.
- Liu Z, Kiessling F, Gatzens J. Advanced Nanomaterials in Multimodal Imaging: Design, Functionalization, and Biomedical Applications. *J Nanomater.* 2010;2010:1-15
- Maeda H. The enhanced permeability and retention (EPR) effect in tumor vasculature: the key role of tumor-selective macromolecular drug targeting. *Advances in Enzyme Regulation*, 2001; 41(1): 189-207.
- Medarova Z, Pham W, Kim Y, Dai GP, Moore A. *In vivo* imaging of tumor response to therapy using a dual-modality imaging strategy. *Int J Cancer.* 2006;118:2796-802.
- Michalet X, Pinaud FF, Bentolila LA, Tsay JM, Doose S, Li JJ, et al. Quantum dots for live cells, *in vivo* imaging, and diagnostics. *Science.* 2005;307:538-44.
- Michela L, Piero F, Federica E, Roberto O, Giovanni L. Current concepts on imaging in radiotherapy. *Eur J Nucl Med Mol Imaging.* 2008; 35:821–837
- Mishra B, Patel BB, Tiwari S. Colloidal nanocarriers: a review on formulation technology, types and applications toward targeted drug delivery. *Nanomed-Nanotechnol.* 2010;6:9-24.
- Molday RS, Mackenzie D. Immunospecific ferromagnetic iron-dextran reagents for the labeling and magnetic separation of cells. *Journal of Immunological Methods.* 1982; 52(3): 353-367.

- Moore A, Basilion JP, Chiocca EA, Weissleder R. Measuring transferrin receptor gene expression by nuclear magnetic resonance imaging. *Bba-Mol Cell Res.* 1998;1402:239-49.
- Mu L, Feng SS. Vitamin E TPGS used as emulsifier in the solvent evaporation/extraction technique for fabrication of polymeric nanospheres for controlled release of paclitaxel (Taxol (R)). *J Control Release.* 2002;80:129-44.
- Mulder WJM, Griffioen AW, Strijkers GJ, Cormode DP, Nicolay K, Fayad ZA. Magnetic and fluorescent nanoparticles for multimodality imaging. *Nanomedicine-Uk.* 2007;2:307-24.
- Muller RH, Wallis KH, Troster SD, Kreuter J. *In vitro* characterization of poly (methyl-methacrylate) nanoparticles and correlation to their *in vivo* fate. *J Control Release.* 1992;20:237-46.
- Murray CB, Kagan CR, Bawendi MG. Synthesis and characterization of monodisperse nanocrystals and close-packed nanocrystal assemblies. *Annu Rev Mater Sci.* 2000;30:545-610.
- National Cancer Institute. BRCA1 and BRCA2. Retrieved on Nov 1, 2010 from the World Wide Web: <http://www.cancer.gov/cancertopics/factsheet/Risk/BRCA>
- National Cancer Institute. Cancer imaging. Retrieved on Nov 1, 2010 from the World Wide Web: <http://imaging.cancer.gov/imaginginformation/cancerimaging>
- National Cancer Institute. What is cancer? Retrieved on Nov 1, 2010 from the World Wide Web: <http://www.cancer.gov/cancertopics/what-is-cancer>.
- Norman ME, Williams P, Illum L. Human serum-albumin as a probe for surface conditioning (opsonization) of block copolymer-coated microspheres. *Biomaterials.* 1992;13:841-9.
- Pan J, Wang Y, Feng SS. Formulation, characterization, and *in vitro* evaluation of quantum dots loaded in poly(lactide)-vitamin E TPGS nanoparticles for cellular and molecular imaging. *Biotechnol Bioeng.* 2008;101:622-33.
- Parak WJ, Gerion D, Zanchet D, Woerz AS, Pellegrino T, Micheel C, et al. Conjugation of DNA to silanized colloidal semiconductor nanocrystalline quantum dots. *Chem Mater.* 2002;14:2113-9.
- Park JH, Lee S, Kim JH, Park K, Kim K, Kwon IC. Polymeric nanomedicine for cancer therapy. *Progress in Polymer Science.* 2008; 33(1): 113-137.
- Peng ZA, Peng XG. Formation of high-quality CdTe, CdSe, and CdS nanocrystals using CdO as precursor. *J Am Chem Soc.* 2001;123:183-4.
- Peracchia MT, Harnisch S, Pinto-Alphandary H, Gulik A, Dedieu JC, Desmaele D, d'Angelo J, Muller RH, Couvreur P. Visualization of *in vitro* protein-rejecting

properties of PEGylated stealth (R) polycyanoacrylate nanoparticles. *Biomaterials*. 1999; 20: 1269–1275.

Prashant C, Dipak M, Yang CT, Chuang KH, Jun D, Feng SS. Superparamagnetic iron oxide - loaded poly (lactic acid)-D-alpha-tocopherol polyethylene glycol 1000 succinate copolymer nanoparticles as magnetic resonance imaging contrast agent. *Biomaterials*. 2010;31:5588-97.

Puisieux F, Barratt G, Couarraze G, Devissaguet JP, Dubernet C. Polymeric micro and nanoparticles as drug carriers. In: Severian D, editor. *Polymeric biomaterials*. New York: Marcel Dekker Inc; 1994. p. 749-94.

Rieter WJ, Kim JS, Taylor KML, An HY, Lin WL, Tarrant T, et al. Hybrid silica nanoparticles for multimodal imaging. *Angew Chem Int Edit*. 2007;46:3680-2.

Ron Hardman. A toxicologic review of quantum dots: Toxicity depends on physicochemical and environmental factors. *Environmental Health Perspectives*. 2006;114(2):165-172.

Roser M, Fischer D, Kissel T. Surface-modified biodegradable albumin nano- and microspheres. II: effect of surface charges on *in vitro* phagocytosis and biodistribution in rats. *Eur J Pharm Biopharm*. 1998;46:255-63.

Sahana D, Mittal G, Bhardwaj V, Ravi Kumar MNV. PLGA nanoparticles for oral delivery of hydrophobic drugs: Influence of organic solvent on nanoparticle formation and release behavior *in vitro* and *in vivo* using estradiol as a model drug. *Journal of Pharmaceutical Sciences*. 2008; 97(4): 1530-1542.

Stolnik S, Illum L, Davis SS. Long circulating microparticulate drug carriers. *Adv Drug Deliver Rev*. 1995;16:195-214.

Sutherland AJ. Quantum dots as luminescent probes in biological systems. *Curr Opin Solid St M*. 2002;6:365-70.

Tada H, Higuchi H, Wanatabe TM, Ohuchi N. *In vivo* real-time tracking of single quantum dots conjugated with monoclonal anti-HER2 antibody in tumors of mice. *Cancer Res*. 2007;67:1138-44.

The Cancer Council of New South Wales. Cancer Myths and Facts: Food preservatives and cancer. Retrieved on Nov 1, 2010 from the World Wide Web: <http://www.nswcc.org.au/editorial.asp?pageid=2345>.

U.S. Food and Drug Administration (FDA). A Fresh Look at Food Preservatives. Retrieved on Dec 10, 2010 from the World Wide Web: <http://www.cfsan.fda.gov/~dms/fdprese.html>.

Van Geuns RJM, Wielopolski PA, De Bruin HG, Rensing BJWM, Van Ooijen PMA, Hulshoff M, et al. Basic principles of magnetic resonance imaging. *Progress in Cardiovascular Diseases*. 1999; 42(2): 149-156.

Wang X, Yang LL, Chen Z, Shin DM. Application of nanotechnology in cancer therapy and imaging. *CA Cancer J Clin.* 2008;58:97-110.

Wang Y, Ng YW, Chen Y, Shuter B, Yi J, Ding J, et al. Formulation of superparamagnetic iron oxides by nanoparticles of biodegradable polymers for magnetic resonance imaging. *Adv Funct Mater.* 2008;18:308-18.

Watters, E. DNA Is Not Destiny. *Discover magazine*, 2006.

Weissleder R, Mahmood U. Molecular imaging. *Radiology.* 2001;219:316-33.

Weissleder R, Moore A, Mahmood U, Bhorade R, Benveniste H, Chioocca EA, et al. *In vivo* magnetic resonance imaging of transgene expression. *Nat Med.* 2000;6:351-5.

Win KY, Feng S-S. Effects of particle size and surface coating on cellular uptake of polymeric nanoparticles for oral delivery of anticancer drugs. *Biomaterials.* 2005;26:2713-22.

Xie J, Chen K, Huang J, Lee S, Wang JH, Gao J, et al. PET/NIRF/MRI triple functional iron oxide nanoparticles. *Biomaterials.* 2010;31:3016-22.

Yan GP, Robinson L, Hogg P. Magnetic resonance imaging contrast agents: Overview and perspectives. *Radiography.* 2007; 13 (Supplement 1): e5- e19.

Zhang Z, Feng SS. Nanoparticles of poly(lactide)/vitamin E TPGS copolymer for cancer chemotherapy: synthesis, formulation, characterization and *in vitro* drug release. *Biomaterials.* 2006;27:262-70.

Zhou J, Sun Y, Du XX, Xiong LQ, Hu H, Li FY. Dual-modality *in vivo* imaging using rare-earth nanocrystals with near-infrared to near-infrared (NIR-to-NIR) upconversion luminescence and magnetic resonance properties. *Biomaterials.* 2010;31:3287-95.

CHAPTER 8: APPENDIX

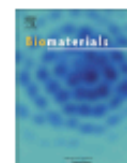
Biomaterials 32 (2011) 296B–297B



Contents lists available at ScienceDirect

Biomaterials

journal homepage: www.elsevier.com/locate/biomaterials



Multimodal tumor imaging by iron oxides and quantum dots formulated in poly (lactic acid)-D-alpha-tocopheryl polyethylene glycol 1000 succinate nanoparticles

Yang Fei Tan^a, Prashant Chandrasekharan^a, Dipak Maity^b, Cai Xian Yong^c, Kai-Hsiang Chuang^c, Ying Zhao^d, Shu Wang^{d,e}, Jun Ding^b, Si-Shen Feng^{a,f,g,*}

^a Department of Chemical & Biomolecular Engineering, Faculty of Engineering, National University of Singapore, 4 Engineering Drive 4, Singapore 117576, Singapore

^b Department of Materials Science & Engineering, Faculty of Engineering, National University of Singapore, 7 Engineering Drive 1, Singapore 117574, Singapore

^c Laboratory of Molecular Imaging, Singapore Biomaging Consortium, Agency for Science, Technology and Research Singapore, 11 Biopolis Way,

#02-02 Helix, Singapore 138667, Singapore

^d Institute of Bioengineering and Nanotechnology, 31 Biopolis Way The Nexus, #04-01 Singapore 138668, Singapore

^e Department of Biological Science, National University of Singapore, 14 Science Drive 4, Singapore 117543, Singapore

^f Division of Bioengineering, Faculty of Engineering, National University of Singapore, 9 Engineering Drive 1, Singapore 117574, Singapore

^g Nanoscience and Nanoengineering Initiative (NUSNN), National University of Singapore, 2 Engineering Drive 3, Singapore 117581, Singapore

ARTICLE INFO

Article history:

Received 10 December 2010

Accepted 31 December 2010

Available online 22 January 2011

Keywords:

Biodegradable polymers

Cancer nanotechnology

Magnetic resonance imaging (MRI)

Molecular imaging

Multifunctional nanoparticles

Nanomedicine

ABSTRACT

This work developed a multimodal imaging system by co-encapsulating superparamagnetic iron oxides (IOs) and quantum dots (QDs) in the nanoparticles of poly (lactic acid) - D- α -tocopheryl polyethylene glycol 1000 succinate (PLA-TPGS) for concurrent imaging of the magnetic resonance imaging (MRI) and the fluorescence imaging to combine their advantages and to overcome their disadvantages as well as to promote a sustained and controlled imaging with passive targeting effects to the diseased cells. The QDs and IOs-loaded PLA-TPGS NPs were prepared by a modified nanoprecipitation method, which were then characterized for their size and size distribution, zeta potential and the imaging agent encapsulation efficiency. The transmission electron microscopy (TEM) images showed direct evidence for the well-dispersed distribution of the QDs and IOs within the PLA-TPGS NPs. The cellular uptake and the cytotoxicity of the PLA-TPGS NPs formulation of QDs and IOs were investigated *in vitro* with MCF-7 breast cancer cells, which were conducted in close comparison with the free QDs and IOs at the same agent dose. The Xenograft model was also conducted for biodistribution of the QDs and IOs-loaded PLA-TPGS NPs among the various organs, which showed greatly enhanced tumor imaging due to the passively targeting effects of the NPs to the tumor. Images of tumors were acquired *in vivo* by a 7T MRI scanner. Further *ex vivo* images of the tumors were obtained by confocal laser scanning microscopy. Such a multimodal imaging system shows great advantages of both contrast agents making the resultant probe highly sensitive with good depth penetration, which confirms the diagnosis obtained from each individual imaging. With therapeutics co-encapsulation and ligand conjugation, such nanoparticles system can realize a multi-functional system for medical diagnosis and treatment.

© 2011 Elsevier Ltd. All rights reserved.